In-Situ Investigation of Particle Assisted GaSb Nucleation Using Environmental TEM

Student: Aidas Urbonavicius

Supervisors: Robin Sjökvist, Miķelis Marnauza and Kimberly Dick Thelander

June 8, 2023

LUNDS UNIVERSITET

Acknowledgements

I am deeply grateful for Kimberly Dick Thelander for giving me the possibility of doing my master thesis together with her research group. It was a great experience working with such a smart and ambitious group of people. I would also like to extend my gratitude to Robin Sjökvist and Miķelis Marnauza for helping me during the experiments and giving me valuable feedback during the writing of this thesis.

I would like to thank Sebastian Lehmann and Pau Ternero for depositing the seed particles on the samples used during the experiments. I am also grateful to Daniel Madsen for helping out and making sure we did not break the ETEM during the experiments.

Also special thanks to all of friends who always supported me during the process of writing this thesis. You always believed in my abilities and my work which helped me immensely. I would also like to thank my parents and my cat Lulu for keeping me sane during the tough times.

Abstract

III-V semiconductor material based nanowires have been extensively studied and shown to be a very exciting building block for future electronics. Material systems such as GaSb show a lot of promise in optoelectric and thermoelectric generation applications because of its high electron mobility and small bandgap. Although there is a lot of research about III-V nanowires, a gap in understanding antimony based nanowire growth is present. The surfactant effect of Sb makes growth of antimony based nanoowires challenging. The aim of this master thesis is to investigate direct nucleation of GaSb from both Au and Sn seed particles which would help to develop a method for direct nucleation. The study is carried out in an environmental transmission electron microscope which enables the nucleation of GaSb to be studied and recorded *in-situ*. Au seeded nucleation occurred at high amounts of Ga present in the particle, above 90 at.%, whilst it is shown that Sn seeded nucleation is possible for a very broad range of seed particle compositions, between 12 at.% and 70 at.%. The Au seeded nanowires were much bigger than the Sn seeded, 100 to 200 nm and 25 to 50 nm respectively, which is related to the Ga amount in the seed particle. This shows that Sn seeded GaSb direct nucleation gives much more promise if the nanowires would be integrated into electrical devices where smaller diameter nanowires are needed. For Au seeded GaSb nanowires twin planes were observed in the zinc blende crystal structure which indicated a possibility of polytypism in GaSb nanowires which has not been reported yet. The observation of polytypism in GaSb is the first step to crystal phase engineering in GaSb nanowires which could be crucial in applications such as nanowire quantum dot devices. This thesis serves as a guideline and a starting point for further GaSb direct nucleation, nanowire growth and crystal structure studies.

Contents

1 Introduction

Throughout history of electronic devices and electric components it has always been the goal to try and manufacture them as small as possible. Once the scale reached nanosize it was observed that materials did not follow the models which have been used for bulk materials. Because of the high surface to volume ratio in nanostructures, surface effects have a big impact which in turn affects how stable the structure of said component is and its properties. Thus a new field of science, nanotechnology, emerged which within scientists study the different phenomena and properties of materials at the nanoscale. One of the most exciting material compounds which have shown to have much promise are III-V semiconductor materials. The III-V material can be either p- or n-doped which allows for precise adjustments of the electrical properties for the desired application. Specifically III-V semiconductor nanowire structures, which are comprised of group III and V elements in the periodic table, have been shown to have many applications in different fields of science, which will be further discussed [1].

The nanowires are 1D nanostructures with a diameter in range from several nanometers to 100 nm, whilst the length can be much longer in range of microns. III-V nanowire nanostructures are in the forefront of nano-technology due to their excellent optical and electrical properties, making them perform well in applications such as photonics, electronics and even quantum computing [2][3][4][5].

One of the most common ways to manufacture nanowires is by growing them directly on a crystalline substrate from a seed particle. It can be done either in a solution or a gaseous environment where a stable nucleus can form on the substrate-particle interface and initiate nanowire growth. The direct growth of nanowires relies on the different growth rates in specific directions in order to achieve the nanowire form. The most common branch of this technique is to use a metal seed particle as a nucleation point. The particle-substrate interface acts as a preferential nucleation site whilst the particle itself can act as a material accumulation point. Particle assisted grown nanowires are not easy to use in devices and are intricate, but have a broader choice of materials, can be grown on different substrates and/or moved onto other surfaces [1].

Most of nanowire manufacturing is done in reactor chambers, where growth parameters are set and the manufacturing process takes place. It is only possible to observe the sample before and after the growth, which means that the whole process is a black box which contains information about the nanowire growth process. This leads to a lot of trial and error in order to find the right parameters for a successful growth, which is ineffective and wastes material. In order to understand what happens in the black box, a method for investigating and observing nanowire growth is needed. An environmental transmission electron microscope is a very useful tool, which gives possibility to grow nanowires inside of the microscope with real time observation and analysis of the nanowire growth. This helps to understand how nanowires grow, as well as give indication on what factors and why affect the resulting structure.

Since the first successful nanowire growth of III-V materials, antimony has been an interesting element to investigate, since antimonide-based nanowires have useful properties such as a narrow bandgap, high electron mobility and highly applicable thermoelectric properties. This makes them suitable for thermoelectric generation applications and high speed - low energy consumption optoelectronic devices. Despite all the exciting possibilities antimonide nanowires have not been studied as much as other III-V materials [6].

Antimony has been shown to act as a surfactant element which in turn can affect the growth mode of semiconductors, crystal ordering, growth of nanowire layers and impede direct nucleation from a seed particle. Studies show that the seed droplets which have incorporated antimony do not form a high enough contact angle and is expected to affect the surface energy balance which might not promote epitaxial nucleation and instead drag the particle along the surface of the substrate [6]. In order to minimize the unwanted effects a stem synthesised from another material is used. For example GaSb nanowires can be grown on a GaAs stem [7]. By using a stem you can only grow a hetero-structural nanowire meaning that you have an interface between the two different materials, which reduces the usability in applications where a structure of a single material is needed. Understanding how to achieve direct nucleation would allow the user to achieve exact composition and structure they are trying to create.

GaSb nanowires are important and useful as p-type semiconductors since GaSb exhibits an intermediate bandgap together with the highest hole mobility in III-V materials. Unfortunately, whilst growing GaSb nanowires using a Au catalyst film it leads to drastically lower hole mobility than the theoretical value [8]. In order to achieve higher hole mobility in GaSb nanowires Sn metal catalyst films instead have been used. By using Sn as a catalyst they improved the hole mobility immensely since the Sn atoms which incorporated into the nanowire acted as dopants [9]. This was observed for surfactant assisted chemical vapour deposition, but there has also been a study which show the similar results but in particle assisted growth [10]. This is only relevant if the application of the nanowires require a high hole mobility, since the doping can not be accurately controlled in current growth setups.

Tornberg et al. has shown that GaSb can be directly nucleated by using Sn seed particles on a GaSb(111)B substrate [7]. An important find they made was that the growth of the GaSb nanowires is highly limited by the nucleation process, which is why further research into nucleation and how other seed materials behave is needed. One way to investigate the nucleation process is through *in-situ* studies, where it is possible to see how the seed particle behaves before and during nucleation as well as how it affects the resulting structure. This makes *in-situ* studies highly important, since during *ex-situ* growth such dynamical processes are unobservable.

AlSb is another antimonide-based III-V material that could be useful for nanowire applications, for example optoelectronics, nanophotonics and quantum processing. It has an indirect bandgap which could be useful in tuning different parameters of optoelectronic devices [6]. Unfortunately there is virtually no research published about successful AlSb axial nanowire growth, only core-shell structures where the core is made of one material which is surrounded by an AlSb layer [11]. Al is prone to oxidation which means that exposure to oxygen could destroy the nanostructure. After *ex-situ* growth the AlSb nanowire structures would have to be capped in order to protect it from oxygen. By investigating the growth and nucleation processes of AlSb nanowires *in-situ* it would be possible to see if successful growth of AlSb nanowires is achievable without capping the nanowire.

2 Goal of the Project

The goal of the project is to achieve direct nucleation of GaSb nanowires *in-situ*. This includes performing nucleation experiments with Au and Sn seed materials and analyzing the nanowire growth *in-situ* by using an environmental transmission electron microscope. The first important analysis is of the seed particle before and during nucleation. By identifying how much of Ga and Sb is absorbed by the seed particle in their respective experiments it is possible to determine optimal nucleation conditions. Structure and behaviour during growth will be identified, studied and explained by analyzing the nanowire structure in different stages of the growth. This is crucial information that is missed during *ex-situ* growth, for example how parameters like precursor flows, partial pressures and temperature can affect nucleation and further nanowire growth. Initially the secondary objective was to investigate the possibility of AlSb nanowire growth. Unfortunately it was not possible because of several problems with the TMAl setup, but two attempts were made to grow AlSb on top of Au-seeded GaSb nanowires. The AlSb experiments did not provide substantial results thus it will be only shortly discussed in the results and outlook part of the thesis.

3 Theory

This chapter presents and explains the theory that the experiments are based on. Firstly metal organic chemical vapor deposition and thermodynamics of nucleation will be discussed, as well as basic principles of semiconductor growth and nanowire nucleation. After presenting the mechanism of nucleation, both the conventional and the environmental transmission electron microscope will be discussed. Lastly the characteristic X-rays, their detection and analysis methods are presented.

3.1 Metal Organic Chemical Vapor Deposition

Metal organic chemical vapor deposition (MOCVD) is a technique used to grow semiconductors and semiconductor structures by using metal organic (MO) precursors or hydrides which deliver the target element to a substrate. Precursors are composed of the target atom and organic groups, such as three methyl groups together with one gallium atom creating

tri-methyl-gallium (TMGa). An alternative to metal organic precursors can be hydrides where the target atom is bonded with three hydrogen atoms, for example arsenic (AsH_3). Figure 1 presents a basic schematic of the MOCVD system.

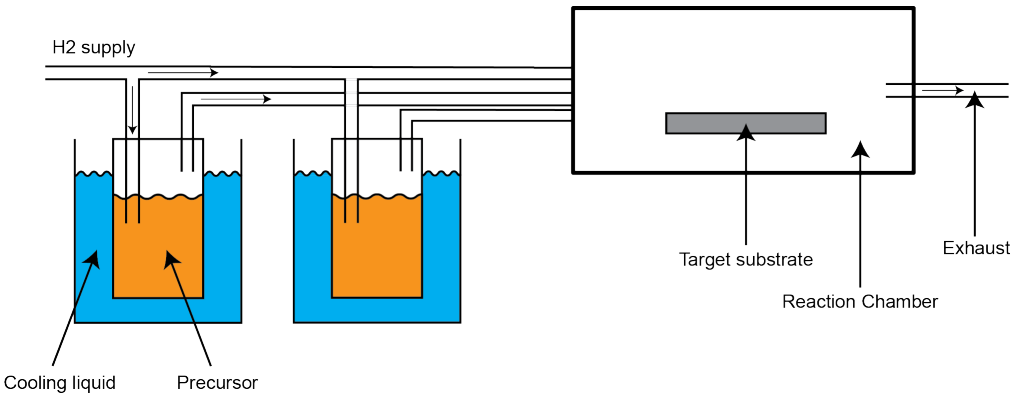

Figure 1: Schematic of a basic MOCVD setup, with the H_2 gas supply, two bubblers - one for group III and one for group V materials, reactor and the connecting gas lines.

The precursors are transported to the system from the bubblers which are temperature-controlled containers filled with the MO. A carrier gas, usually H_2, is pumped through the bubbler where the carrier gas bubbles are able to saturate with the MOs and transport it to the reaction chamber through pipes and pressure controllers. If the temperature is high enough in the reactor chamber, MO will undergo pyrolysis and release the atom which can then diffuse on the surface of the substrate, adsorb or remain in the gas phase. The pyrolysis process is relatively simple but since it does not only depend on the temperature but also pressure, surface and its composition and interaction with other precursor molecules, it can be quite tricky to exactly estimate the pyrolysis efficiency. What is most important is that the precursors do undergo pyrolysis and successfully deliver the desired atom to the reactor for it to be able to participate in the growth/deposition. Precursors which have several organic groups, such as TMGa, undergo pyrolysis in several different steps by dissociating one methyl group at a time. Once the precursors have pyrolysed and the target material is in the reactor chamber, it can start forming compounds and

creating semiconducting material or structures on the crystalline substrate [12].

3.2 Thermodynamics of Nucleation

In order for the elements to form a crystal/semiconducting material, first a small conglomerate of the said elements have to arrange themselves in a small structure - a nucleus. Creation of a stable nucleus is directed by the change in Gibbs free energy and the difference in chemical potentials of metastable phase, in this case ambient environment and the stable phase which is the liquid nucleus as depicted in Figure 2. If the Gibbs free energy change is positive it means that the process is thermodynamically unfavorable, otherwise a negative change results in a favourable process, as seen in Figure 3. The change in Gibbs free energy is composed of three different influence terms: volume ΔG_V, phase boundary area ΔG_S and elastic stress term ΔG_E.

$$\Delta G_N = \Delta G_V + \Delta G_S + \Delta G_E \tag{1}$$

To nucleate, first the ambient environment has to be saturated with the material. This means that the concentration of material in the ambient environment has to reach the solubility limit. Once the concentration is above the solubility limit, it is supersatured, the ambient phase becomes metastable thus it is thermodynamically preferred to create a nucleus, which is the stable phase. The creation of a nucleus will lower the total energy of the system and will keep growing as long as the ambient environment is above solubility limit which is the driving force for nucleation and growth. The volume change term in the Eq.1 is negative because it is a favorable process since the new stable phase will lower the systems energy by reducing the volume of the metastable ambient phase. This is counteracted by the phase boundary term which is the interface between metastable and the stable phase. It is proportional to the interface area between stable and metastable phases and is positive since creation of a surface requires energy. If the nucleus experiences elastic stress, then the elastic stress terms becomes positive and counteracts the negative volume term. For this general case discussion an unstrained nucleus is considered [12].

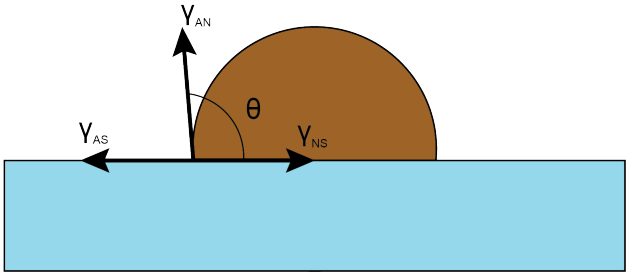

Figure 2: Schematic of the nucleus, which can be either a solid or a liquid, substrate and ambient environment surface energies.

There is a size dependent balance between the contribution from the volume term and the surface term. When a small nucleus forms, if the volume is too small the total change in Gibbs free energy will be positive thus the nucleus will break down, since the negative volume term is small. If the volume of the created nucleus is large enough, then the negative volume term will be bigger than the surface term thus making the nucleus stable. The size of the nucleus where the change in Gibbs free energy is at its peak is called the critical nucleus radius, which is denoted r* in Figure 3. If the radius is too small, then increase in radius will increase Gibbs free energy which is not favorable. If the radius is larger then increase in nucleus radius will lower the Gibbs free energy thus creating a stable nucleus which can start growing, which is seen in Figure 3 [12].

There are several different growth modes possible depending on how surface energies relate to each other. This is described by Young's relation:

$$\gamma_{AS} = \gamma_{NS} + \gamma_{AN} cos\theta \tag{2}$$

where γ_{AS} is the surface energy for ambient-substrate interface, γ_{NS} is the nuclei-substrate interface, γ_{AN} is the ambient-nuclei interface and θ is the wetting angle. The surface energies together with the wetting angle determine if the nucleus formation is three-dimensional or two-dimensional.

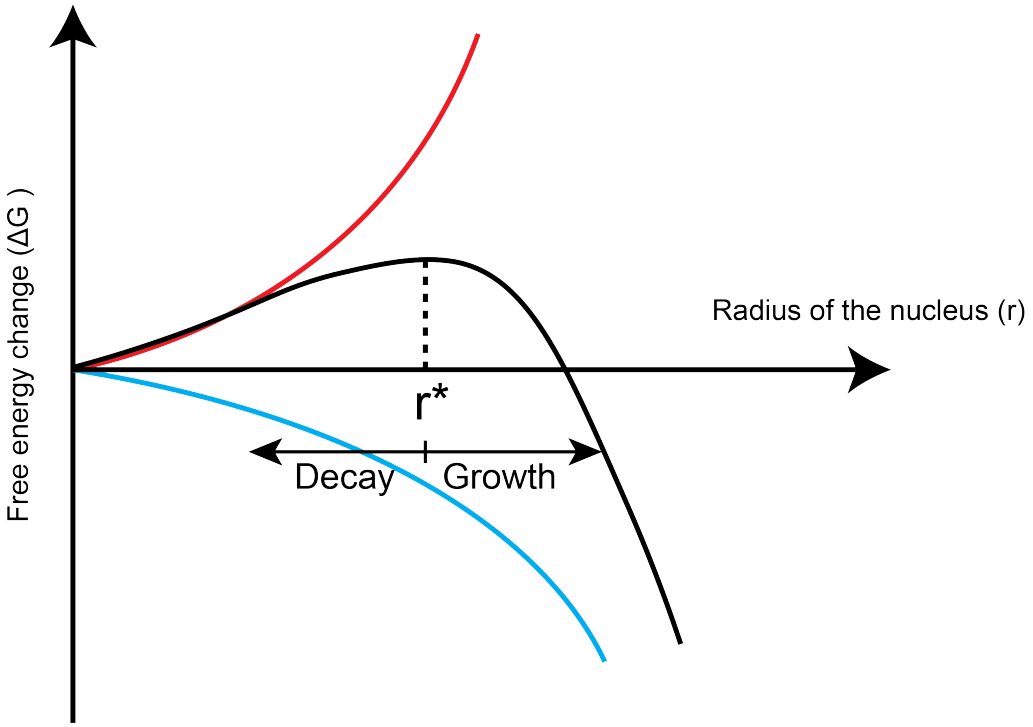

Figure 3: A sketch of Gibbs free energy change with varying radius of the nucleus. The volume term curve is blue and the interface surface is red.

If the γ_{AS} is greater than the sum of γ_{AN} and γ_{NS} it means that it is preferred to minimize ambient-substrate surface thus inducing layer growth which is called Frank van der Merve growth regime. If the γ_{NS} surface energy is higher, then the system will try to minimize the surface between the substrate and the nucleus, inducing island growth. The regime for island grow is called Volmer-Veber. The third regime is called Stranski-Krastanov growth where the first layers are grown by Frank van der Merve growth regime until it reaches a critical layer thickness, where then the next layers are formed by Volmer-Veber. This results in island growth. The reason for it is that the layers growing after the critical layer thickness will experience strain which in turn affects the energy balances [12]. This is a general description, where the ambient environment can be either a gas or a solution. For further discussion only the gaseous phase is considered together with a liquid seed particle.

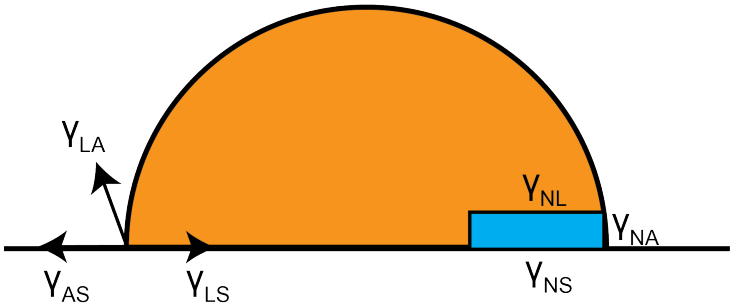

Figure 4: Schematic of the seed particle which is in an ambient gas environment and has a small nucleus. The new surface energies of the nucleus are noted in the schematic.

In order to understand nanowire nucleation, a three phase system has to be considered: the ambient phase, particle phase and the substrate phase which is depicted in Figure 4. The nucleus can either form on the triple phase line or in the middle of the nanowire-substrate interface. For this scenario only the triple phase line nucleation will be considered, since nucleation without a nucleus-ambient surface has not been yet observed *in-situ*. When a nucleus forms, it will introduce several new surface energies: nucleus-liquid (NL), nucleus-ambient (NA) and nucleus-substrate (NS). Note that the droplet is not the nucleus anymore, thus the surface energies are γ_{AS}, γ_{LA} and γ_{LS} where L stands for liquid. Depending on the new surface energies, it will determine if the nucleus continues to grow or breaks up. One important difference is that when a solid nucleus forms the surface to the substrate there can be a lattice mismatch which would induce strain on the nucleus. Then the elastic stress term from Eq. 1 comes into play, which is a positive term thus making nucleation less thermodynamically preferable. But after the critical layer thickness, the next layers nucleus will form an interface on the first layer which will have the same structure meaning that there will be no elastic stress present for the new nuclei. This suggests that it is harder to form the first few layers, but it will be progressively easier to grow succeeding layers.

3.3 Particle Assisted Nanowire Growth

The first nanowire like Si whiskers were grown by using an impurity droplet which gave the idea for experiments of nanowire growth by using a metallic seed particle as a starting point for the nanowire growth which is schematically depicted in Figure 5 [13]. To this day metallic, especially gold, nanoparticle seeds are one of the most universal and most used in seeded nanowire growth [14].

In order to grow nanowires, metallic seed particles are deposited on a crystalline substrate which can alloy with the supplied elements in the system, for example by using MOCVD. Once nucleation conditions are fulfilled which are dependant on gas flows and temperature, a small nucleus forms. The interface between the particle and the nucleus is where the new layers of the wire will form as shown in Figure 5. The nucleation and growth can follow the vapour-liquid-solid (VLS) mechanism or vapour-solid-solid (VSS) mechanism depending on the phase of the seed particle.

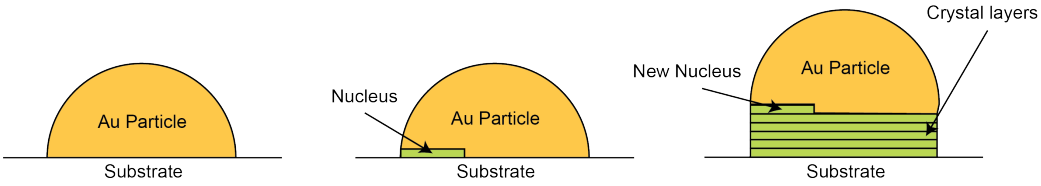

Figure 5: Schematic of particle assisted nanowire growth, from left to right, from the seed particle on the substrate to the first nucleus forming and then succeeding layers which form the nanowire.

As stated previously, MOCVD is a quite common method of particle assisted nanowire growth. The process of nucleation from a metallic seed particle inside of the MOCVD reactor chamber is summarized in Figure 6. Materials that are supplied to the chamber are in gas/vapour phase which then start alloying with the seed material at elevated temperatures. Once the seed particle reaches the limit of the solubility it will be in the equilibrium state. If even more material alloys with the particle, it will shift from equilibrium thus becoming supersaturated. Since the particle is not in equilibrium, the alloying materials will have to leave the seed particle thus precipitating a solid nucleus in order to reach the equilibrium

concentration. This does depend on the surface energies and change in Gibbs free energy which means that the particle has to be quite above the the equilibrium conditions in order to overcome the kinetic energy barrier of nucleation. Once the particle has nucleated, the amount of material needed in the seed particle becomes less since now there is a nucleus present on which the growth can continue. Since nucleation is the first step which requires the seed particle to reach higher saturation than equilibrium state, it is important to study and understand. In order to continue the growth, appropriate amount of material has to be provided in the gas phase so that it can continue alloying with the seed particle and reach the supersaturation levels, which are lower than for nucleation. This means that the the growth conditions are not the same as nucleation conditions, so typically one has to adjust the gas flows in order to optimize the growth conditions after nucleation [1].

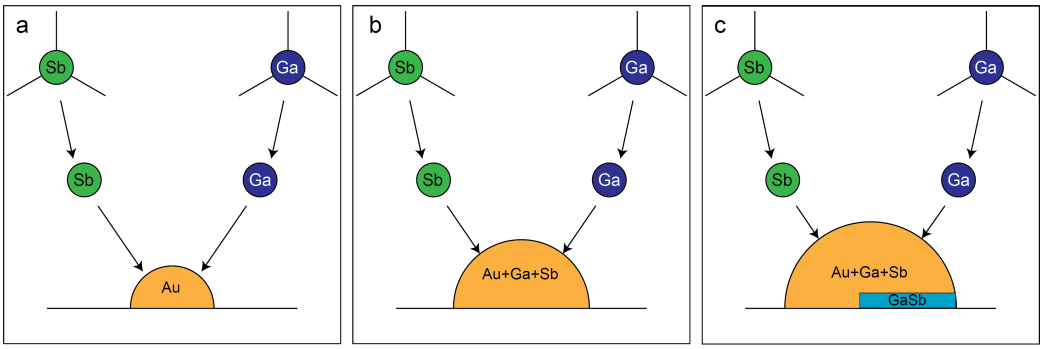

Figure 6: Basic schematic showing the particle assisted nucleation in a MOCVD reactor chamber. First the precursors pyrolyse and release the target atom which can alloy with the seed particle (a), then as more material alloys with the particle it increases in size and is starting to reach supersaturation (b), once the supersaturation is reached a small stable nucleus forms (c).

There are several theories related to the role of the metal particle as a catalyst for nanowire growth. The precursor molecules which arrive to the chamber have to pyrolyse to release the target atom. Higher temperatures increase the rate of which the molecules pyrolyse but it is also speculated that they do pyrolyse faster at the seed particle surface. Thus, higher local

concentration of the material around the seed particle is present, which leads to a higher chance of it alloying with the seed particle and reaching supersaturation faster. Besides the particle acting as a catalyst itself, it is also possible that the interface between the substrate and the particle can create a more favoured area for nucleation. That is because the particle can act as a material sink which means that a higher Ga concentration is present in the particle than in the vapor, especially at the surface of the substrate thus the driving force for nucleation is highest under the particle [1].

3.4 Crystal Structure of III-V Nanowires

Some of the most common materials for nanowire growth are GaN, GaAs and InAs which are used in optoelectronics, as a catalyst or in quantum-dot applications [15][16][17]. Most of III-V bulk semiconductor materials grow in a zinc blende (ZB) crystal structure, except nitrides which usually have a wurtzite structure (WZ). When it comes to III-V nanowires, surprisingly most of the non-nitrides can grow in both ZB and WZ structure, but even higher polytypes such as 4H or 6H [18]. The stacking of group III and V elements in the nanowire determine the crystal structure. For ZB the atoms stack in 3 different layers (ABCABC) which is depicted in Figure 7 lower panel and is a cubic structure, whilst WZ has only 2 different stacking layers (ABAB) and is a hexagonal structure as seen in Figure 7 upper panel [18]. An important difference between ZB and WZ is that they exhibit different sized bandgaps. The direct bandgaps are somewhat similar, whilst indirect bandgaps can vary a lot, about 1 eV [19]. The different sized bandgaps of WZ and ZB structures are important to study, since they can create crystal heterostructures which be used for nanowire quantum-dot growth. A small ZB part of the nanowire is grown in between WZ structures where there is a sharp interface between ZB and WZ which can confine electrons, thus forming a quantum-dot [20].

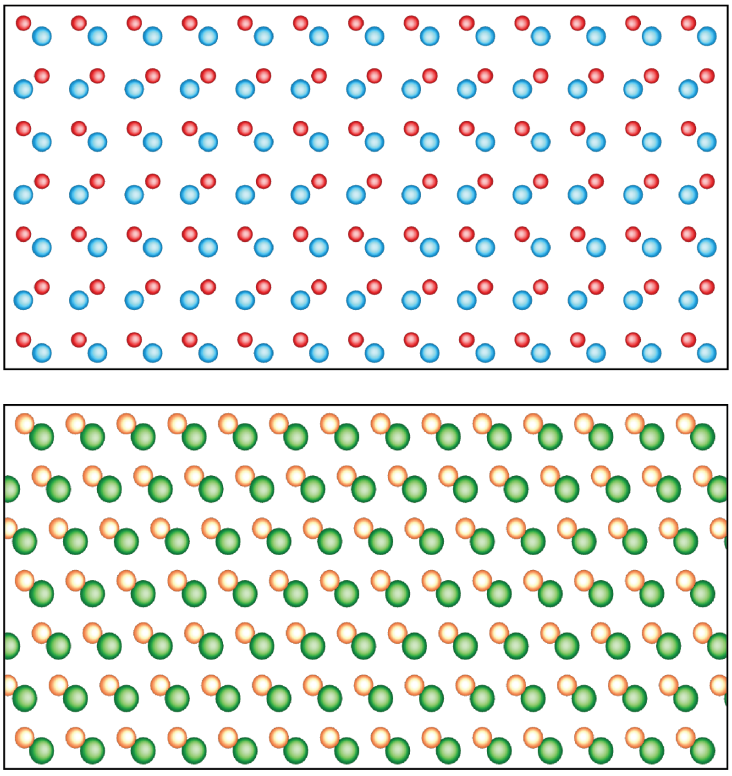

Figure 7: Model of atomic stacking in WZ crystal structure is shown in the upper panel where the viewing direction is $[11\bar{2}0]$ of the [0001] growth direction (upwards in figure). The atomic stacking of ZB crystals structure is shown in the lower panel where the viewing direction is $[1\bar{1}0]$ of the [111] growth direction (upwards in figure).

3.5 Transmission Electron Microscope

To study materials at the nanoscale the conventional optical microscope does not have the sufficient resolution since the wavelength of photons is too large. Instead, electrons are used in order to achieve better spatial resolution. Transmission electron microscope (TEM) takes advantage of electrons which have a shorter wavelength compared to photons and uses them for imaging. TEM uses a parallel beam of electrons that usually is accelerated to the range of 80-300 keV. Figure 8 presents different parts of the TEM, which will be referred to throughout this chapter.

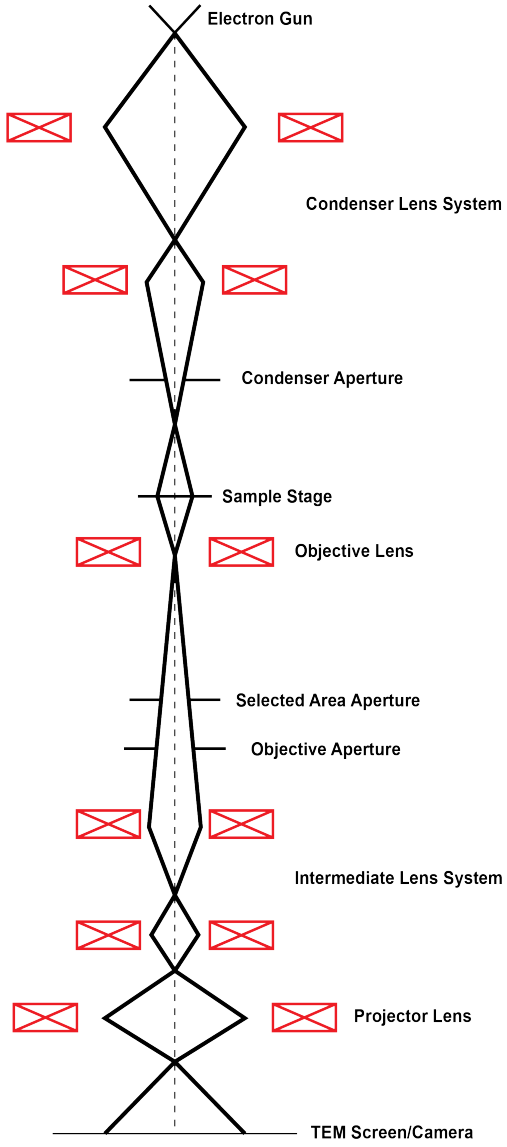

Figure 8: A schematic showing fundamental parts of the TEM.

3.5.1 Electron Source

To understand how electrons are generated and accelerated it is important to understand how the electron gun works. There are different types of electron guns used in the TEM: thermionic, Schottky and field emission

[21].
The thermionic electron gun is made of a material which has a high melting point such as tungsten (W). High energy electrons of the conduction band of the W filament cannot leave the surface since much higher energy is required to remove an electron to vacuum. The difference between the vacuum and solid surface energy is called the work function of the material which acts as a potential barrier. At high enough temperatures, the electron can leave the surface since the thermal energy is enough to overcome the work function and release the electron into vacuum. In order to overcome the work function, a high current is applied over the W filament which heats it to high temperatures, around 2700K. An alternative to W is a material that would have a lower work function which would not require as high temperatures. Lanthanum hexaboride (LaB_6) is a common alternative to W, which has a lower working function and only needs to be heated to 2000K [21][22].

The Schottky electron gun is a W thermionic emitter but is coated with zirconium oxide in order to lower its work function. An electrostatic field is applied over the covered tip of the filament and an extractor, which has a positive bias compared to the filament tip, is used to apply an accelerating voltage over the tip itself. This results in a higher current density, compared to LaB_6, but needs much better vacuum since zirconium oxide is easily contaminated [21][22].

The field emission electron gun is based on the quantum-tunneling phenomenon. By applying an electric field over the filament the potential barrier becomes sufficiently small so that there is a possibility for electrons to tunnel through the surface potential barrier. Since the thermal energy is no longer required, the field emission electron gun can be used in room temperature, thus called cold field emission gun. A high vacuum is needed in order to keep the tip clean, but if the current becomes unstable because of adsorbed gases or other particles on the tip it is possible to quickly increase temperature which removes the impurities from the surface of the tip - so called flashing [21][22].

The electrons that overcome the work function of the electron gun filament do not have the required accelerating voltages of 80-300 keV. In order to accelerate the electrons an anode, which is a metal plate with a

circular opening in the center just below the filament tip, and the electron gun, which acts as a cathode, is used. The emitted electrons pass the plate and because of the immense voltage difference are accelerated [21][22].

3.5.2 Lens Systems in the TEM

Once the electrons reach the desired acceleration voltage it is important to be able to control the spread of electron beam and how much of the sample is illuminated. This is controlled by using the condenser lens system, see Figure 8. Magnetic lenses are not perfect and suffer from optical aberrations which mean that the electron beam is not perfectly focused. Besides the lenses there are tools such as stigmators which adjust for the different aberrations. Two different magnetic lenses are used : Condenser lens 1 and 2 (C1 and C2). C1 controls the magnification of the electron beam and determines the size of the focused/defocused beam, so called spot size. C2 has no magnification, but allows to vary the area of the sample which is illuminated. In order to control the angle of what electrons pass through the lens an aperture is placed in C2 which limits the angle of the passing electrons. The aperture can be moved around in order to center it around the electron beam optical axis since high angle electrons are harder to focus and can contribute to abberations. Both C1 and C2 have stigmators placed after them in order to further adjust the beam and remove any axial astigmatisms [21][22].

After the beam focus and spot size is adjusted, another system of magnetic coils is used in order to shift and/or tilt the electron beam. The system consists of two different pairs of coils, where one of them can control the beam shift in x and y axis, whilst the other can tilt the beam by changing the angle between the incident beam and the optical axis [21][22].

Now that the beam has been adjusted accordingly it can finally illuminate the sample which is placed in a sample holder, also called the specimen stage, see Figure 8. Since there is vacuum inside of the TEM, it is important that when loading the sample the vacuum is not broken. An airlock is used in order to remove air from around the sample holder which then can be inserted into the vacuum environment. The sample holder can be differently equipped in order to give it tilting ability which makes possible

to tilt the sample in either one or both axis, as well as provide heating [21][22].

During the electron beam transmission through the sample, it interacts with sample and gets scattered. The scattered electrons enter the imaging lens system which is comprised of an objective lens, intermediate lenses, projector lens and their respective apertures and stigmators, see Figure 8. The image of the sample is created by using the objective lens. The objective aperture can be placed in the back focal plane (BFP) of the objective lens where the diffraction pattern (DP) is formed. By adjusting the size of the aperture it is possible to choose electrons which have a specific angle or lower to let through, whilst electrons which are diffracted at higher angles get blocked. The blocked electrons are not detected thus look like a dark area in the image, whilst the electrons which pass through appear bright thus creating a contrast. If there are any astigmatism which arise from the lenses, the stigmator can be used to correct it. A selected-area aperture can be placed in the image plane in order to choose a specific area of the specimen. This makes it possible to achieve a DP of a small area of the sample [21][22].

Before the image can be formed on the TEM screen it has to go through the intermediate lens system. The main purpose of the intermediate lens system is to magnify the image and/or move the BFP onto the TEM screen in order to form a DP. The magnification is adjusted by varying the lense currents in small increments which in turn change their focal length. In order to bring the BFP onto the screen more substantial changes in lens current are required. The last lens is called the projector lens which forms the actual image on the TEM screen [21][22].

3.5.3 Electron Beam Interaction With The Sample

There are two different ways an electron from the electron beam can interact with the atoms present in the sample - either by interacting with the nucleus or atomic electrons. Since nuclei are positively charged the incoming electron will interact according to electrostatic Coulomb forces. When the electron travels close to the charged nuclei, it will experience an attraction force which will change the trajectory of the electron - the electron gets scattered. This sort of scattering is considering elastic, since

the electron preserves all of its kinetic energy, only changing its direction. If the beam electron travels too close to the charged nuclei it will change its direction drastically. The change in direction can result in an emitted x-ray, thus this sort of scattering would be considered inelastic and the x-rays are called Bremstrahlung radiation. If instead the incoming beam electron interacts with the atomic electron, there will be repulsion forces between them since they are both negatively charged. This results in energy loss thus the electron interaction is deemed to be inelastic. Besides categorizing electrons into elastic/inelastic, they can undergo either coherent or incoherent scattering. Coherent scattering is when the electron waves are in the same phase and the same wavelength, whilst incoherent waves do not have any of these relations. Elastically scattered waves are mostly coherent, whilst inelastic are incoherent [21][22].

3.5.4 Contrasts in the TEM

In order to describe how close an electron has to pass by a nucleus in order to be affected, a scattering cross section is defined as an area that describes the probability of an incoming electron interacting with the nucleus. It has circular form since the nuclei are spherical. When calculating the probability for a bulk material, not for a single atom, it is shown that the calculations have to include both the thickness of the sample and the nuclei size which depends on the atomic number Z. Thus the difference in sample thickness and Z will give rise to different angles and amounts of electron scattering creating a mass-thickness contrast in the images. This is the most prevalent contrast in amorphous materials and the electron scattering is considered to be incoherent elastic scattering [21][22].

Materials that are crystalline or poly-crystalline have atoms arranged in a specific order - a lattice which forms a crystal plane. Depending on how the crystal plane is oriented relatively to the incoming beam, the electrons from the electron beam will scatter differently. Since there are many crystal planes present, the scattered electron waves will thus interfere with each other. This is called diffraction. In order to describe the diffraction phenomena Braggs law is used:

$$n\lambda = 2dsin\theta_B \tag{3}$$

where λ is the wavelength of the electron, θ is the Braggs angle which

is defined as the angle between incoming electron beam and the specific lattice plane, d is the distance between two atomic planes and n is an integer. This explains how the reflected electron waves from atomic planes diffract relative to the incoming electron wave. If the difference of the angles match the Braggs angle, the diffracted electron wave will thus create a high intensity spot in the back focal plane (BFP). The pattern of all the different interferences is called the diffraction pattern (DP). By studying the diffraction pattern it is possible to determine the wavelength of the incoming electron wave (if the crystal structure is known) or the atomic spacing (if the wavelength is known). DP is one of the main methods which crystalline samples are studied since it gives crucial information about the crystal structure and the inter-atomic spacing [21][22].

Diffraction contrast in TEM images arises from electrons which have scattered without losing energy and retain their phase, are elastic and coherent, and scattered at Bragg angles. There are two different ways to choose how to construct the image: dark-field and bright-field. Bright-field imaging mode is when the objective aperture is positioned such that only the direct transmitted electron beam pass through which appears bright in the image. If the aperture is placed such that only electrons which have diffracted at specific or all higher angles are able to pass through but the main beam is blocked off, then it will result in a dark-field image. The default imaging mode from TEMs is bright-field, but instead of only selecting the transmitted beam, low angle diffracted electrons pass through as well and form the image [21][22].

Phase contrast arises from the diffracted electron waves and incoming beam electron waves interaction. The electron waves with different phases will interfere with each other thus creating a contrast in the image. If the crystal is positioned such that the crystal planes are parallel to the incoming beam, it will give possibility for high resolution imaging in the TEM (HRTEM) at high magnifications. By using HRTEM imaging it is possible to achieve atomic resolution images. That is why it is important to have a sample holder which can be tilted, so that the crystalline material/structure can be oriented such that atomic resolution is achievable. Another result of phase contrast are Fresnel fringes which form around the edges of objects in the TEM image. This can be used to determine if the sample is in focus or out of focus. Also depending on the contrast of the Fresnel fringe it is

possible to learn if the image is under or over focused [21][22].

Best practical resolution in the TEM is achieved when the electron experiences one scattering event when traveling through the material. Otherwise multiple scattering events degrade the resolution of images and diffraction patterns. That is why only samples of up to 200 nm thickness are used in the TEM since thicker samples induce more scattering events thus making it more difficult to interpret. Rule of thumb is that the sample must be thinner than 100 nm to achieve atomic resolution images [21][22].

3.6 Environmental Transmission Electron Microscope

An environmental TEM (ETEM) is a setup where several different parameters such as temperature, pressure, gas composition and/or electrical/magnetic fields can be adjusted inside of the TEM to carry out *in-situ* studies allowing investigation of nanomaterials and nanoparticles in a dynamic environment. This allows to image, study and analyze different materials in environments that are otherwise impossible to realize using conventional microscopy methods. It can be used for example to study phase transition of different materials during temperature changes, nanowire growth kinetics or investigation of nucleation and layer growth in nanowires [23][24][25]. Without the help of an ETEM these processes would have been difficult to study which signifies the importance of *in-situ* studies.

There are two different methods that can be used to expose a sample to environment changes in an ETEM - in a closed-cell or an open-cell configuration. In a closed cell, there is a small isolated chamber where the sample can be placed in and then the whole chamber is placed inside of the TEM. The chamber has a small thin window on the top and the bottom, either made from carbon or silicon, which lets the electron beam through. The chamber has a gas inlet and an outlet where the gas can be supplied into, but it is also possible to create an enclosed gas and/or liquid environment that can instead be static during the studies in the ETEM, and instead only parameters such as temperature can be varied. The small reactor volume which is contained only around the sample and is not exposed to the microscope column means that much higher flows and pressures can be realised [26].

An open-cell configuration means that the whole TEM column becomes the reactor chamber which is exposed to gases and the sample is just fitted inside of the holder which is then inserted into the column. This requires extra vacuum pumping in the TEM column, especially close to the gun chamber, see Figure 9 where 3 different ion pumps (IP1,2,3), dry rotation pump (DRP) and a turbo-molecular pump (TMP) are installed. If the material in the gas phase is not pumped away in the vicinity of the electron gun, the material will be deposited on the gun thus rendering it unusable. That is the main limitation of an open-cell configuration - it is only possible to achieve a certain pressure around the sample without disrupting the electron gun. That is why it is problematic to directly compare results from the ETEM to *ex-situ* since *ex-situ* MOCVD reactors have much higher pressures and flows.

Closed-cell configuration has several limitations compared to open-cell. The range of available tilt is much smaller for closed-cell than open-cell configurations since the window in the cell is quite small and tilting the holder would mean that the window alignment would shift thus not letting the electron beam through. Sample tilt is quite important, especially when studying crystalline materials, such as III-V nanowires, as it allows for the sample to be tilted into a low index crystal direction thus giving atomically resolved images. Another limitation is that it is really hard to achieve a reasonable amount of counts to perform X-ray energy dispersive spectroscopy analysis. The sample is encased in a chamber made of many different materials and the characteristic X-rays can simply not penetrate it and reach the detector. Even if it could, the signal would be quite muddled with all the extra X-rays emitted from the window and the reactor chips. It is important to choose the right configuration for a certain experiment, as the two different approaches have very distinct and drastic differences. This is why open-cell configuration is much more attractive for nanowire growth *in-situ* studies, it provides better images and compositional data as well as allowing for crystal structure analysis.

One type of an open-cell ETEM is a setup where a MOCVD gas system, see Figure 1, is coupled with a TEM to carry out *in-situ* studies. By combining these two techniques it is possible to observe and study nanowires during growth which is otherwise missed during *ex-situ* growth. Dynamic

effects like layer-by-layer growth, incubation and step flow, crystal growth mechanics, seed particle composition during nucleation are very important and relevant for nanowire growth studies, which is why an ETEM coupled with a MOCVD system is a crucial tool in the field.

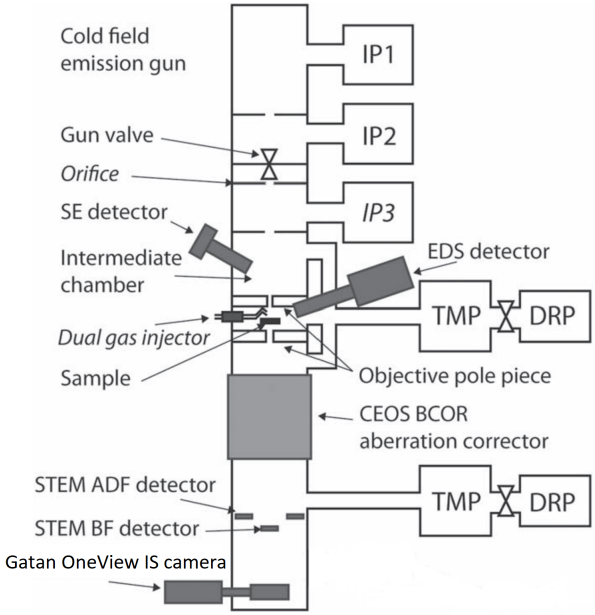

Figure 9: Schematic of the ETEM in nCHREM which is used for *in-situ* studies where the sample is exposed to different gas compositions. Figure adapted with permission from Hetherington et al. [27]

One of the biggest advantages of *in-situ* studies is that the parameters such as pressure or temperature can be varied while observing the sample. This gives possibility of adapting the parameters according to what is observed during the experiment. *In-situ* research can be used as guidelines for *ex-situ* growth which could save a lot of time and reduce the number of failed growth experiments.

3.7 Energy Dispersive X-ray Spectroscopy

When the electrons from the electron beam interact inelastically with inner shell core electrons of the material being studied they can eject the

inner shell electrons. Once an electron is ejected the atom can return to the lower energy state by one of the outer shell's electrons filling the hole left in the core shell.

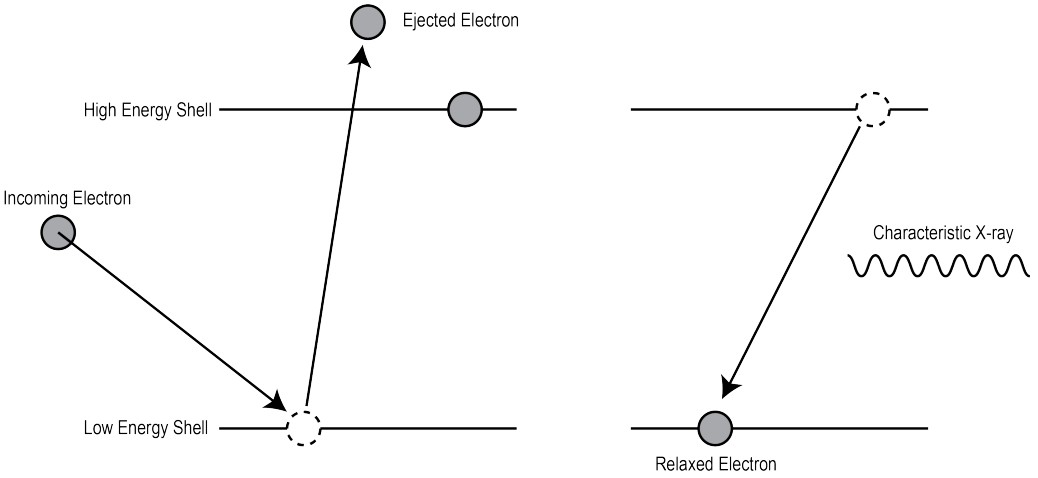

Figure 10: Basic schematic of how characteristic X-rays are emitted. The incoming electron ejects the lower energy shell electron. An electron from a higher energy shell will relax into the hole left thus emitting a characteristic X-ray.

Since the outer shell electron fills the now empty state the atom can relax, which can result in either an emitted X-ray or an Auger electron, see Figure 10. An Auger electron is another electron which gets ejected by the result of the relaxing electron transferring the energy to it. The emitted X-ray has the energy of the difference between the two different energy states which are specific to the element thus is called characteristic X-rays. Characteristic X-rays give information about what elements are present in the sample as well as gives opportunity to do quantitative calculations [21].

In order to eject the inner shell electrons, the electrons which come from the beam have to have higher energy than that of the difference of the two energy levels – critical ionization energy. Different elements have different amounts of protons in the nucleus thus the electrons are bound differently. Increasing amount of protons means that the electrons are more tightly bound and are closer to the nucleus, so the energy which is needed to excite the inner shell electrons is much higher. When the ejected electron leaves

the atom and a higher energy electron fills the hole, there are several possible ways a higher energy state electron can fill the hole. These combinations of which shell the relaxing electron drops from is what results in the XEDS spectrum as different types of peaks which are called families. There are vast amount of different possibilities, but the most prevalent are K, L and M families which have the highest intensity. The energy resolution of the XEDS detectors is not sufficient for resolving many low intensity peaks that are generated which means that they are rarely used. Also there is a lot of peak overlap for the lower energy families making identification and quantification problematic [21].

Quantitative XEDS analysis is most commonly performed by using the Cliff-Lorimer ratio:

$$\frac{C_A}{C_B} = k_{AB}\frac{I_A}{I_B} \tag{4}$$

Where A and B are two different elements, I_A and I_B is the peak intensity, C_A and C_B is weight percent and k_{AB} is the Cliff-Lorimer factor which is not constant. The k factor depends mostly on what accelerating voltage one uses and the microscope/XEDS setup. By using the Cliff-Lorimer ratio equation it is possible to achieve quantification of different elements in the spectrum by using their peak intensities and the k factor, either in weight or atomic percentage [21].

Most common type of XEDS detectors are semiconductor based, such as Si or Ge, but there are some calorimetry based which are rarely used [28]. The emitted X-rays hit the XEDS detector which is comprised of many different channels and gets transformed into an electrical charge pulse by using electron-hole pairs. The pulse then gets converted to a voltage which in turn gets amplified and recorded as a digital signal. Different X-rays give rise to different pulses which can then be sorted out and a spectrum of different energies can be formed. Most of the charge pulses come from the characteristic X-rays, but it is not the only way the detector can create a charge pulse. Temperature can activate the electron-hole pairs present in the detector thus creating a noise signal which can muddle the desired characteristic X-ray signal. Even at room temperatures the noise signal can be relatively high, which is why it is important to cool the XEDS detector. Most of the common ways is either to use liquid nitrogen or water, depending on the desired quality of the XEDS analysis [21].

XEDS also gives the possibility to perform temperature calibration by using the strobe peak. Strobe peak is the result of thermally emitted X-rays from the sample, which directly correlates to the temperature. By analyzing and comparing the strobe peak intensity and shift it is possible to determine the current temperature of the sample. This is quite useful if the samples one wants to use differ in shape, thickness or other properties. In order to do this one has to have a reference spectrum where the temperature is known which other measured spectra can be compared to [29].

4 Experimental Methods

This chapter presents the experimental methods, used equipment and materials for the experiments. The processes of making, depositing and characterising the two different seed particles are explained, as well as how the experiments were conducted.

4.1 Equipment

All the experiments were done in the Hitachi HF-3300S ETEM at nCHREM which is integrated to a MOCVD gas handling system. Video and image capturing was done in TEM mode by Gatan OneView IS camera. The composition was analyzed by using XEDS and the metal organic and hydride precursors were supplied by the connected gas handling system. Amorphous silicon nitride (SiN_X) Micro-electro-mechanical system chips (MEMS) with deposited seed particles were used as the starting point for nanowire nucleation. Most of the data analysis was performed by using Digital Micrograph software, ImageJ, Aztec and Matlab.

All quantification of XEDS analysis was done by using Aztec. It uses Cliff-Lorimer ratio (see Eq. 4) and theoretical k-factors according to their manual.

The MEMS chips from NORCADA have 4 gold heating contacts which are connected to a tungsten heating coil which surrounds the SiN_X substrate. The substrate has 19 circular areas where there is a thin SiN_X film with a circular hole in the middle as depicted in Figure 11. Particles which

were deposited on the thin SiN_X were studied during all the experiments. Particles were analyzed by using XEDS analysis.

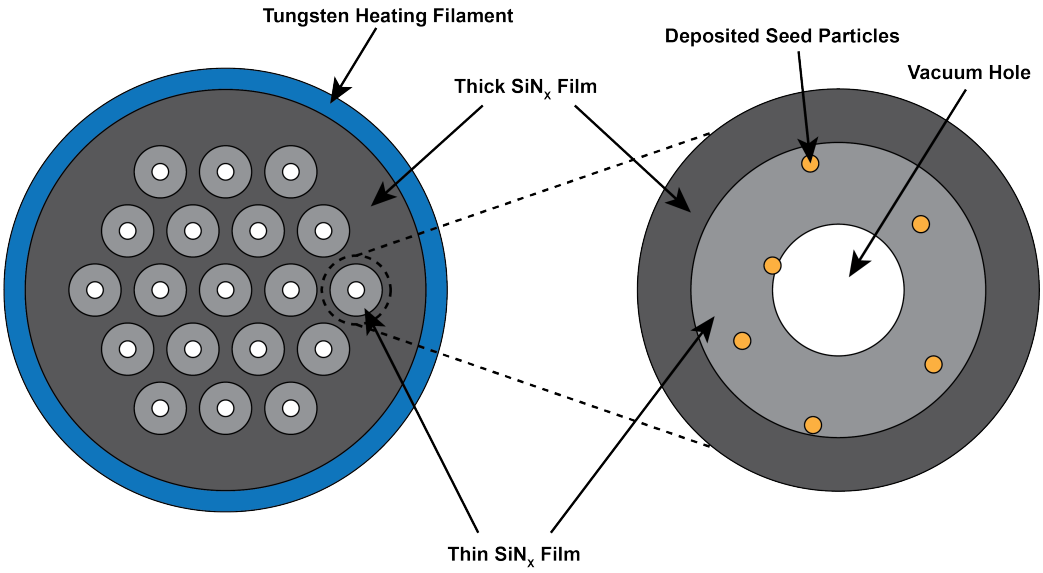

Figure 11: Schematic of a NORCADA MEMS chip and a zoomed in schematic of the holes in which seed particles are deposited on.

4.2 Gold Particle Deposition

Gold nanoparticles of 30 nm were deposited on the MEMS chip with density of 1 particle per square micron, see Figure 12 right panel. The particles were deposited by using size-selected nanoparticle aerosol technology. The basic principle of the aerosol deposition is that pure gold is vaporized which then gets carried away by nitrogen gas through a furnace. Once the particles leave the furnace, they fuse together and form bigger particles. The particles pass several differential mobility analyzers which classify the particles by their diameter which then are deposited on the MEMS chip [30][31]. The size and composition of the seed particles were confirmed with TEM and XEDS analysis.

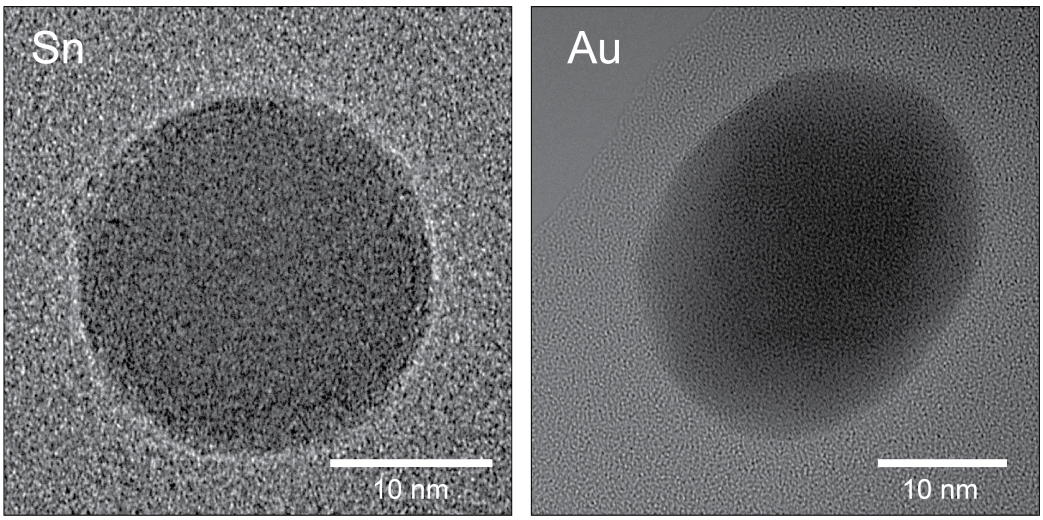

Figure 12: Images of a gold particle (right) at 420°C and a tin particle (left) at 145°C before any gasses were introduced into the system

4.3 Tin Particle Deposition

Tin particles were deposited on the MEMS chip by using spark ablation. High voltage was applied over the target material by using two metal pieces, anode and cathode, as the metal sparks small particles are formed. The particles agglomerated to bigger particles and were carried away by a carrier gas nitrogen which then got deposited on the MEMS chip. Particles size varied from 20 to 25 nm and were deposited with 2 particles per square micron density, see Figure 12 left panel. Size and composition were confirmed by using the TEM and XEDS analysis.

5 Results and Discussion

Relevant results and discussion of the different experiments are presented in this chapter. Main focus is on the nucleation, but also other interesting findings and their relevancy is discussed. In the end of the chapter there is a comparison of the two different seed particles and what different results were achieved by using them.

Table 1: Summary of all the experiments in chronological order.

Experiment #	Summary of the experiments
Au #1	Achieved nucleations at high amounts of Ga in the seed particle.
Au #2	Reproduction of Au #1 on the same chip with Ga preloading, but with several contamination issues.
Au #3	Further reproduction of Au #1 on a new chip, temperature induced nucleation.
Sn #1	Observations from Au experiments used to nucleate at much lower amounts of Ga.
Sn #2	Reproduction of Sn #1 and electron beam induced nucleation.

5.1 Gold Seeded Results

In this section experimental results are presented from the three different experiments, see Table 1. The results are discussed in the chronological order that they were performed.

5.1.1 Nucleation Methods

All the partial pressures and seed particle compositions from the first experiment (Au #1) are plotted in Figure 13 and will further be referenced throughout this chapter. The Au #1 experiment was started by introducing both TMGa and TMSb into the system at the same time at partial pressures $4.23 \cdot 10^{-3}$ Pa TMGa and $6.02 \cdot 10^{-2}$ Pa TMSb at 420°C, condition 1 in Figure 13. This did not result in any nucleation and the Ga amount in the seed particle was around 30 at.% , whilst the amount of Sb was 3 at.%. When growing GaSb on GaAs stem the minimum observed amount of Ga is 60 at.%, which means that 30 at.% is likely not enough for the particle to reach supersaturation. Thus TMGa flow was increased, up to $5.79 \cdot 10^{-3}$ Pa partial pressure of TMGa. The increase of TMGa flow lead to more Ga in the Au particle, around 55 at.% but still no nucleation was observed. Since Sb has been shown to affect surface energies [6] which could possibly hinder nucleation, the TMSb flow was lowered which resulted in partial pressure of TMSb of $2.87 \cdot 10^{-2}$ Pa, condition 2 in Figure 13. The amount of both Ga and Sb in the particle increased, Ga increased to about 80 at.% and Sb to

6 at.%. These conditions still did not yield any nucleation. This suggests that the seed particle still has not reached supersaturation, thus TMGa flow was increased and TMSb decreased resulting in partial pressure of TMGa $2.43 \cdot 10^{-2}$ Pa and TMSb $2.91 \cdot 10^{-2}$ Pa which is condition 3 in Figure 13. This resulted in the first observed GaSb nucleation from Au seed particles which is shown in Figure 14.

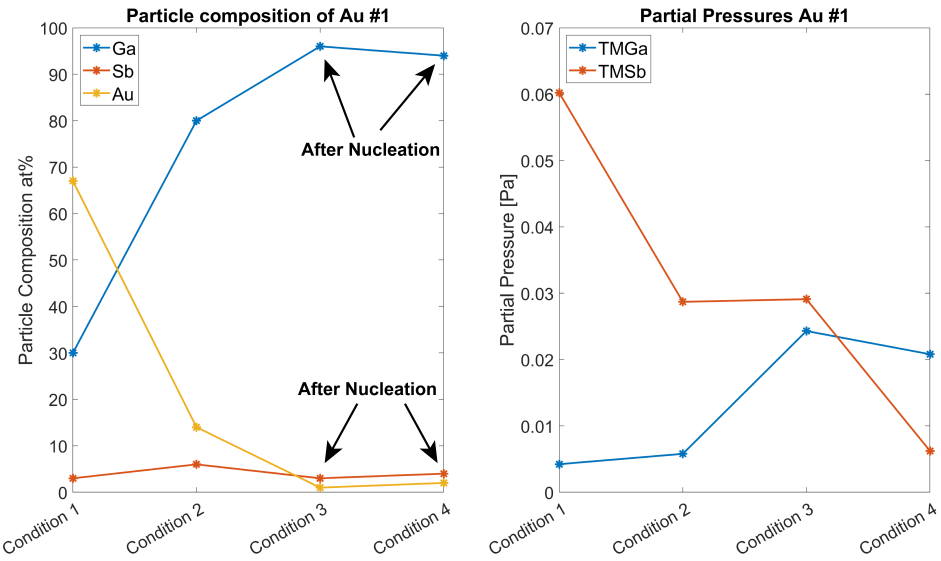

Figure 13: Plot of the Au #1 experiment partial pressures and the composition of the seed particle. All the measurements were taken at 420°C. Note that some of the XEDS data were acquired post nucleation.

The XEDS analysis of the particle showed composition of 96 at.% Ga, 3 at.% Sb and 1 at.% Au. The particle was located at the thick-thin SiN_X interface and it had already started to grow towards the thin part of SiN_X. The particle width was about 151 nm, but a part of the particle was still wetting the thick-thin interface of SiN_X so the diameter of the wire could not be determined. Other particles on the MEMS chip did not seem to have nucleated and the amount of Ga in those particles were about 90 at.%. Since the nucleated particle had 96 at.% Ga in it, TMGa flow was further increased in order to achieve above 90 at.% of Ga in another Au particle. The resulting partial pressure of $2.62 \cdot 10^{-2}$ Pa did not increase the amount of Ga in the particle, which was still at 90 at.% and Sb at 7 at.%. This

suggests that Sb is still preventing Ga incorporation which does not allow the particle to reach supersaturation. Because of this reasoning, TMSb flow was further decreased which resulted in TMGa $2.08 \cdot 10^{-2}$ Pa and TMSb $6.23 \cdot 10^{-3}$ Pa partial pressures which is condition 4 in Figure 13. These conditions lead to more particles nucleating, where the composition of one of the seed particles were measured to be 94 at.% Ga, 4 at.% Sb and 2 at.% Au. This matched the particle composition of the first nucleation observed. The particles and the nanowires were approximately the same size as the first observed nucleated particle, about 150 nm.

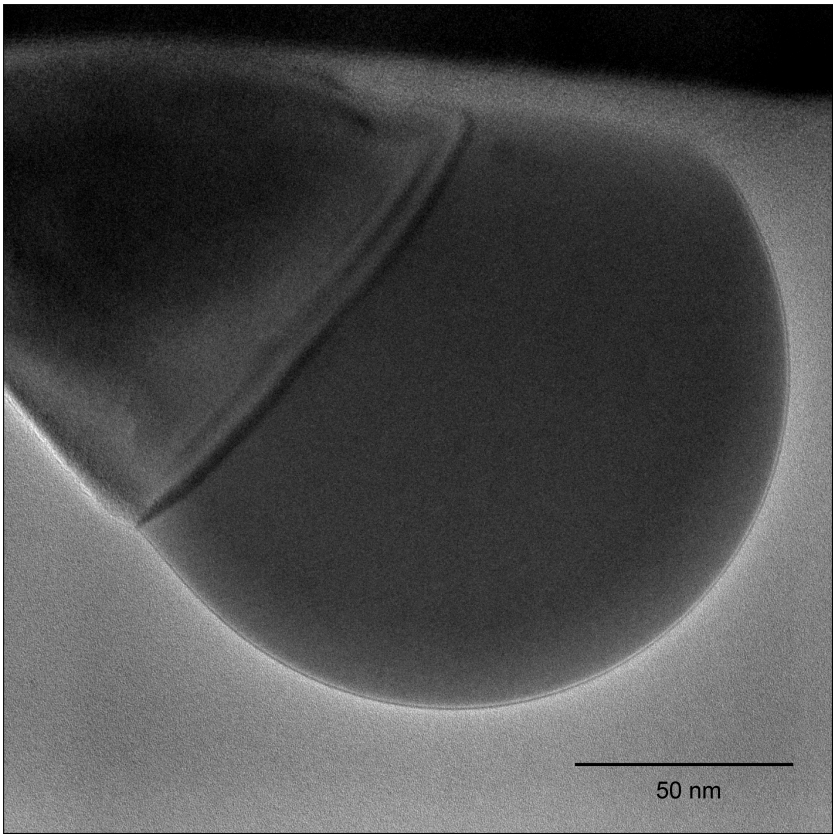

Figure 14: First observed Au seeded nanowire which nucleated and is growing from the thick-thin part of SiN_X.

These results were quite surprising, since it was not expected that such high amounts of Ga were needed in the particle for it to nucleate. Also the

resulting nanowires and the particles increased in size from about 30 nm to 100-200 nm which is quite significant. Thus for the following experiments it was important to reproduce the results from the first experiment whilst also investigating if nucleation at lower Ga amounts in the particle is possible, which could decrease the diameter size of the nanowires. It was noted that higher flow of TMSb in the particle did prevented Ga absorption, so for other experiments only TMGa was introduced into the system first, without any TMSb so that the particles could alloy with Ga faster. This can be attributed to the surfactant properties of antimony, which increases the kinetic nucleation energy barrier by affecting the wetting angle and the surface energies.

Au #2 experiment was started by first introducing TMGa in the system, without any flow of TMSb. Temperature was constant at 420°C during the whole experiment. Once the composition of the seed particle reached 60 at.% Ga, TMSb was introduced in the chamber at partial pressure of TMSb $5.21 \cdot 10^{-2}$ Pa and TMGa $6.09 \cdot 10^{-3}$ Pa which is condition 1 in Figure 15. The choice of 60 at.% Ga was based on the lowest observed amount needed for GaAs-GaSb growth. The composition of the seed particle was measured to 55 at.% Ga, 2 at.% Sb and 43 at.% Au. Since no nucleation was observed, the TMGa flow was increased and TMSb decreased to try and increase the amount of Ga in the seed particle. The flow adjustment led to partial pressures of $1.35 \cdot 10^{-2}$ Pa TMGa and $4.04 \cdot 10^{-3}$ Pa TMSb which is condition 2 in Figure 15. This resulted in the seed particle composition of 63 at.% Ga, 2 at.% Sb and 35 at.% Au. Since no nucleation was observed and the amount of Sb seemed low in the particle, the flow of TMGa was reduced whilst TMSb increased, resulting partial pressures of $6.02 \cdot 10^{-3}$ Pa TMGa and $5.14 \cdot 10^{-2}$ Pa TMSb which is condition 3 and 4 in Figure 15. This still did not result in any nucleation and the particles did not reach higher Ga amount than 90 at.%.

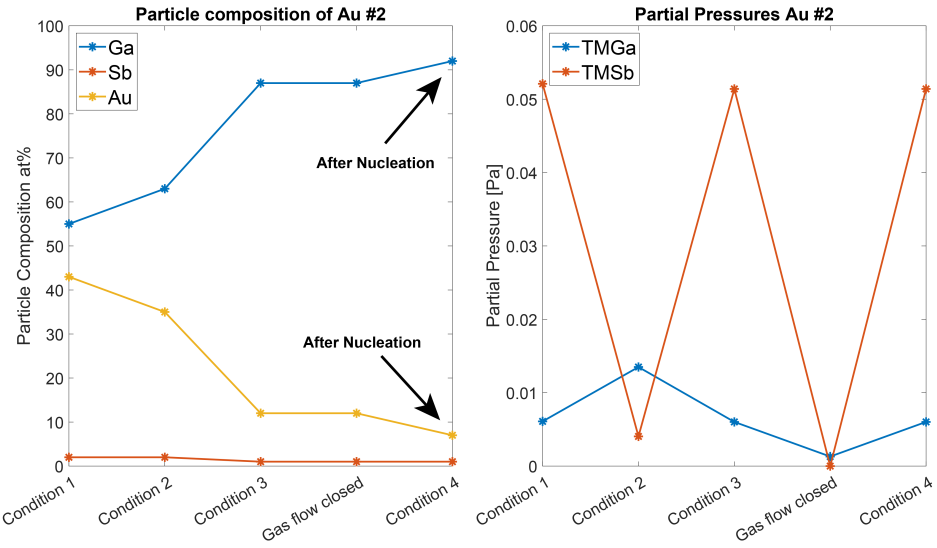

Figure 15: Plot of the Au #2 experiment partial pressures and the composition of the seed particle at temperature 420°C. Note that some of the XEDS data was acquired post nucleation

TMSb flow was stopped in order to see if the amount of Ga increased in the particle. After the gas flow of TMSb was stopped the particles did reach the composition of 92 at.% Ga, 1 at.% Sb and 7 at.% Au. After reintroduction of the TMSb it was observed that several different particles had nucleated, which is shown in Figure 16 panel (a), and even some growing nanowires were found. The first observed nucleated nanowire had the diameter of 88 nm and was growing from the thick-thin part SiN_X interface which is shown in Figure 16 panel (b). Other nucleated nanowires were of similar size.

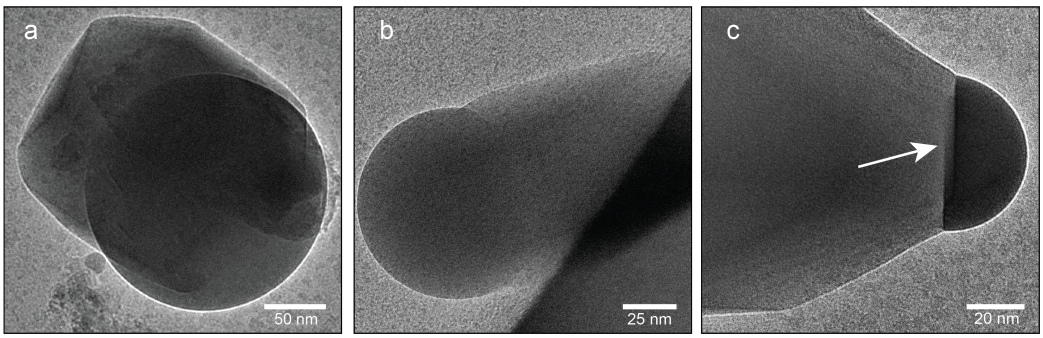

Figure 16: Images of Au seeded nanowires. Image of a nucleated particle shown (a), a nanowire growing from the thick-thin SiN_X interface (b), a tapering nanowire which exhibits multilayer growth as indicated by the white arrow (c).

One particular nanowire which is shown in Figure 16 panel (c) had been tapering down. The bottom part of the nanowire, where the initial nucleation happened, was about 120 nm in diameter whilst the particle was 55 nm wide. The nanowire width decreased more than a factor of two. It is quite hard to assume what conditions resulted in this tapering behaviour since the nanowire was found at the end of the experiment. Nonetheless this might suggest that it is possible to control the diameter of the nanowire by adjusting the Ga amount in the seed particle which directly affects its size. Besides the tapering, the nanowire was still growing when observed and it was growing by multi-layer growth mechanism, as indicated by the white arroes in Figure 16 (c). Multi-layer growth in nanowires has been reported before, but not in GaSb nanowires [32][33].

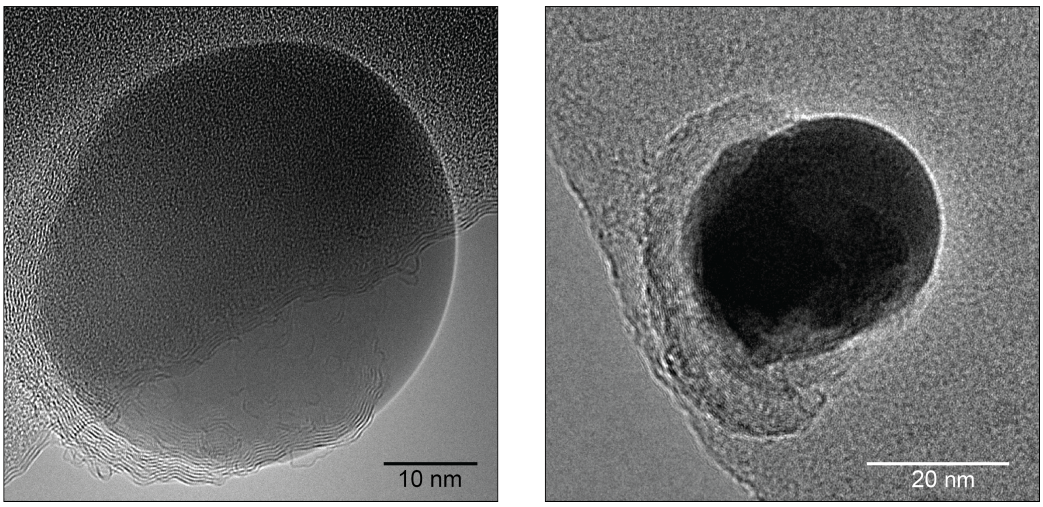

Figure 17: Images of two Au seed particles partially covered in an amorphous shell and graphene layers.

Au #2 experiment was performed on the same MEMS chip as the first experiment. In order to remove any GaSb structures and the nanowires the chip was heated to 750°C overnight. Overnight etching does not perfectly clean the chip so there is a possibility of contaminants still left on the sample. By investigating the chip with TEM no obvious contamination was observed. Despite that, during the experiment most of the seed particles had a partly amorphous shell present around them as seen in Figure 17 left panel. Some of the shell had distinct layers and a structure which is similar to a graphene structure such as in Figure 17 right panel. During the experiment it was clear to see that the shell did not allow the particles to nucleate, because the it acted as capping layer hindering the droplet volume increase thus required supersaturion for nucleation could not be achieved. This could be attributed to contamination, since TMGa and TMSb are used as precursors which have three methyl groups each, so when it pyrolyses it releases three methyl groups per precursor molecule into the system. The high amount of hydrocarbons could be deposited on the chip and around the particles during experiments, and might have been relatively low during the Au #1 experiment, but during the Au #2 experiment it is possible that it continued to form thicker structures.

Because of the contamination issue, a third experiment Au #3 was

performed on a new chip that had not been used to grow or nucleate nanowires before. The goal of the Au #3 experiment was to try and induce nucleation by sequential addition of precursors but on a clean chip. First TMGa was introduced in order to let the Au particles alloy with Ga, without any TMSb present in the system. Once the particle composition reached 91 at.% Ga and 9 at.% Au, the TMSb was introduced which resulted in $5.3 \cdot 10^{-3}$ Pa TMGa and $2.37 \cdot 10^{-2}$ Pa TMSb partial pressures. No nucleation was observed and the particle composition was 86 at.% Ga, 6 at.% Sb and 8 at.% Au. In order to achieve higher amount of Ga in the seed particle the TMGa flow was increased thus changing partial pressures to $1.50 \cdot 10^{-2}$ Pa TMGa and $2.30 \cdot 10^{-2}$ Pa TMSb. Nucleation was observed at these conditions, but only on the thick part of the SiN_X. Since in the previous experiment it was observed that closing and re-opening the TMSb lines lead to increased amounts of Ga in the seed particle, the TMSb lines were closed of and turned on again after 15 minutes. The restarting of gas supply did lead to some nucleation on the thin part of SiN_X, but the majority of the Au particles had not nucleated.

During the experiments, it was quite difficult to find the optimal conditions for nucleation. The general method is to achieve high enough Ga amount in the seed particle, above 90 at.%, then introduce TMSb into the system in order for the particles to nucleate. Otherwise the presence of Sb in the system might alter the surface energies, the contact angle, and the chemical potential which could in turn impede nucleation and reduce the amount of Ga in the seed particle. This method did not seem to be consistent, since only some particles nucleated, mainly on the thick-thin part of SiN_X.

As mentioned in section 3.2, nucleation is achieved by overcoming the solubility limit and reaching supersaturation in the particle which leads to nucleation. This method is based on the change of partial pressures around the seed particle and the chemical potentials of different phases present. An alternative to this is temperature shock. By lowering the temperature quickly it is possible to lower the solubility limit which means that the particle can nucleate at lower amounts of material present in the seed particle [34]. Since the solubility limit falls below the current material concentration which results in high supersaturation, it will be thermodynamically preferable to create a solid crystal phase. Once the

particle has nucleated, the temperature needs to be increased again in order for the nanowire to grow and reduce the risk of contamination deposition on the sample. When the temperature is increased, it will increase the solubility limit back thus making it less thermodynamically stable for the solid crystal phase to exist, which might break up and alloy back to the seed particle [34]. As long as the amount of the material present in the particle was above supersaturation at the initial stage, some of the newly created nucleus will be absorbed back to the particle, but a part of it will stay in the solid phase.

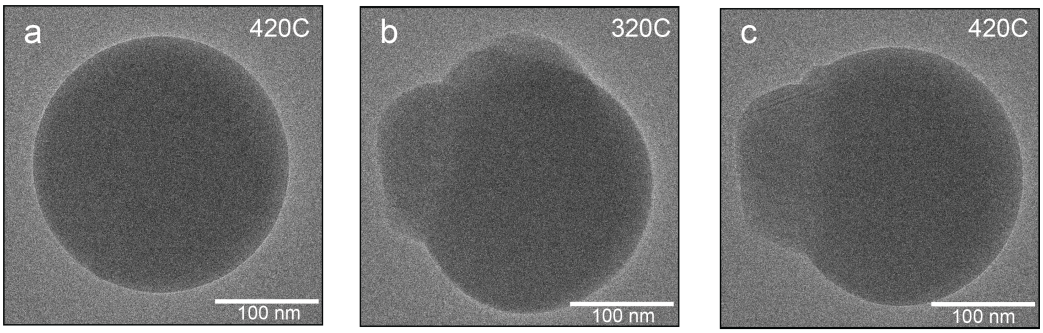

Figure 18: Image of the particle before the temperature decrease at 420°C (a), once the temperature was decreased to 320°C and a nucleus was formed (b), and after the temperature was increased back to 420°C with some of the nucleus still remaining (c).

During the Au #3 experiment a reliable way to achieve nucleation from Au seeded particles by using temperature shock was demonstrated. Before performing the temperature shock partial pressures of $1.96 \cdot 10^{-2}$ Pa TMGa and $2.34 \cdot 10^{-2}$ TMSb Pa were used for the precursor flows similar to experiment Au #1 at condition 3 as seen in Figure 13. A Au-Ga-Sb particle before the temperature shock is shown in Figure 18 panel (a). The seed particle composition before the temperature shock was 86 at.% Ga, 4 at.% Sb and 10 at.% Au which was in a supersaturated state as evident by the increase of the particle volume. To induce temperature shock the temperature was decreased from 420°C to 320°C which resulted in a nucleus formation after 2 s which is shown in Figure 18 panel (b). Once the nucleus was formed, about after 0.5 s, temperature was increased back to 420°C, which resulted in part of the nucleus alloying back into the

particle, but as seen in Figure 18 panel (c), part of it still was in the solid phase. The particle composition was almost the same as pre-nucleation as it was post-nucleation, ±1 at.%. This was successfully performed on several different Au seed particles and is a consistent method of GaSb nucleation from Au seed particles.

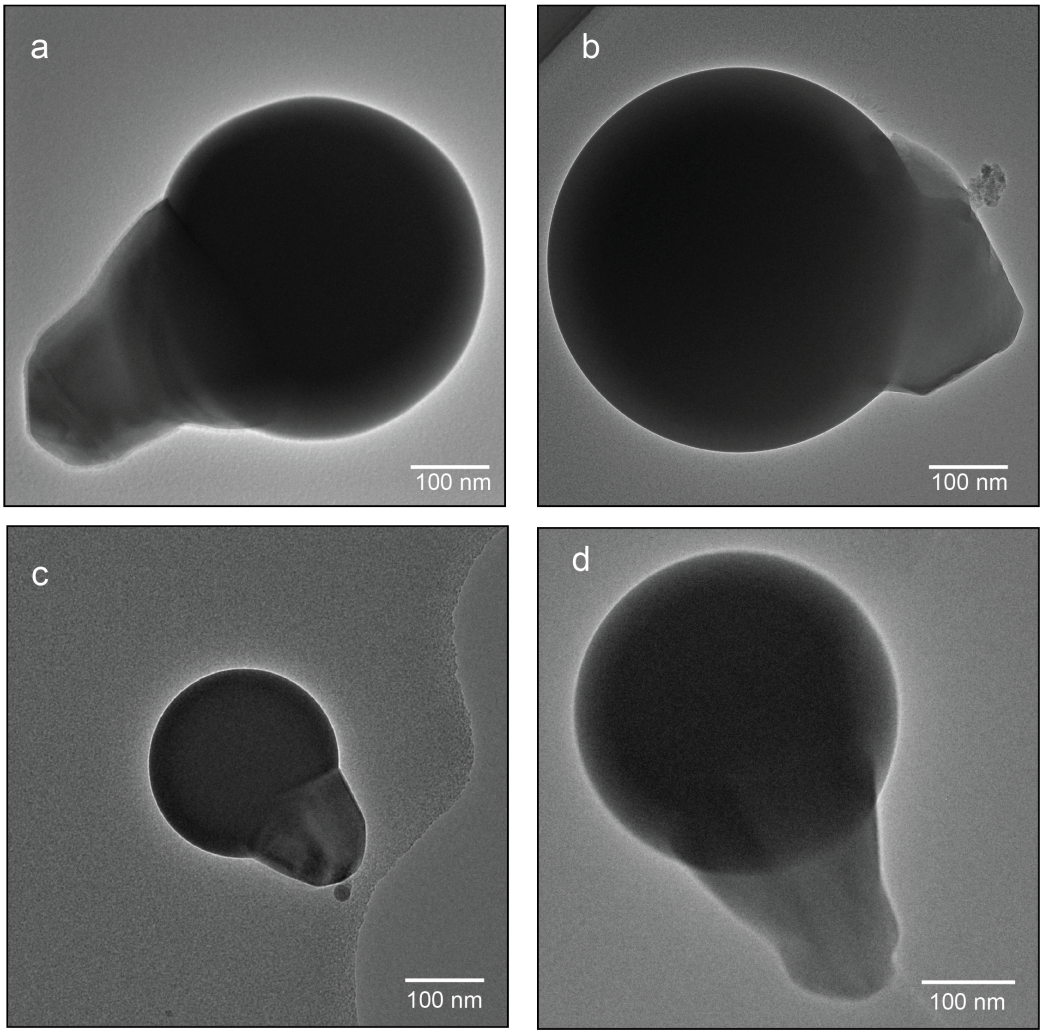

Figure 19: Images of nucleated and growing nanowires from the gold seed particles on the thin SiN_X layer.

During the experiments it was observed that too high amounts of Sb

present in the Au seed particle hindered nucleation and might have even affected how much Ga can be alloyed with the seed particle. This could be attributed to the surfactant properties which have been observed in other material systems. It has been proposed that Sb lowers the chemical potential difference in GaAs nanowires which hinders the formation of WZ crystal structure [35]. This suggests that Sb can also hinder the particle from reaching supersaturation by lowering the chemical potential difference. Only when the particle swells up and increases its Ga amount drastically can it reach the supersaturation and successfully nucleate. Contact angle can also be affected by Sb as it has been observed that GaSb nanowires tend to grow along the surface and do not form nanowires because of the low contact angle. A contact angle of 90°or larger is usually needed for nanowire growth, which could suggest that the contact angle is not high enough thus preventing direct nucleation [6].

5.1.2 Twinning in GaSb Nanowires

Twins were observed in one of the Au seeded nanowires during the Au #3 experiment which is shown in Figure 19 panel (a) and Figure 20. This nanowire was found after the gas supply was closed down so it is hard to tell exactly when or how the twin planes formed. Although, during the experiment most particles were nucleated by temperature induced shock and since the twin plane defect is present at the stem of the wire, it is possible to assume that it formed shortly after the temperature shock nucleation during the time the particle composition was stabilizing.

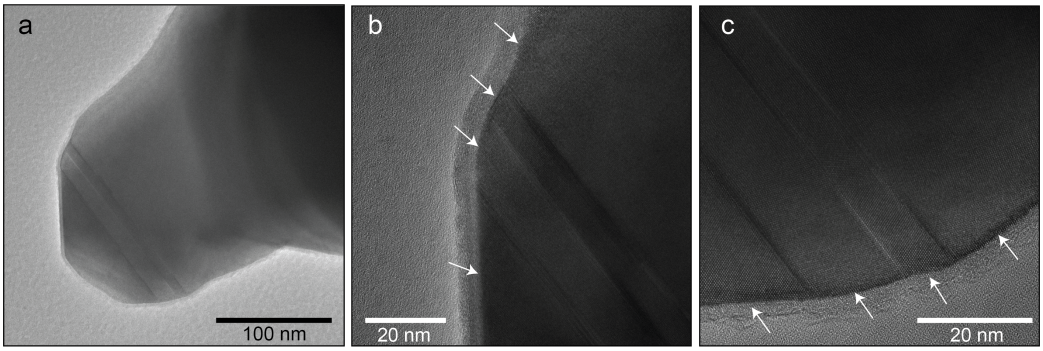

Figure 20: Image of a nucleated nanowire which has a twin plane defect in the stem of the nanowire (a), zoomed in images in the upper and the lower side of the wire (b-c) of the twin planes with visible atomic planes. The white arrows point at the four different ZB segments with the twin planes in between them.

There have been other finds of twins in GaSb nanowires in work by Tornberg et al. who also reported twin plane defects in *ex-situ* growth of GaSb nanowires, but the GaSb nanowires in their experiments were Sn seeded, not Au seeded [7]. One big difference is that the twin planes observed in the work of Tornberg et al. were inclined twin planes, whilst the ones observed in this thesis are parallel to the crystal layers. Ghalamestani et al. has also conducted a study where they investigated if WZ structure is possible in InSb and GaSb [18]. They were successful in forming WZ InSb, not GaSb, but they did observe several parallel twin plane formations in the GaSb nanowires. The twins most likely formed in our experiment during temperature shock, which is when the solubility limit is drastically lowered. Temperature shock can be related to TMSb pulsing which was performed in Ghalamestani et al. work [18]. They suggest that by pulsing TMSb during InSb growth the supersaturation changed for favourable WZ formation. The same TMSb pulsing was performed for GaSb growth which lead to twin planes, thus indicating that TMSb pulsing drastically changes the supersaturation in GaSb. This further suggests that in order to form twin planes or WZ crystal structures in GaSb high levels of supersaturation are needed. It is also noted that high supersaturation is only achievable at very low TMSb flows, which agrees with Ghalamestani et al. *ex-situ* work and several other studies [18].

This is an interesting find since antimonide nanowires almost always

grow as defect free ZB structure and are not expected to have twin planes or any other defects [6]. Since twin planes are occasionally observed before the transition from ZB to WZ, this observation suggests that there is a possibility that GaSb can be grown in other crystal structures besides ZB, such as WZ [36].

5.1.3 Self Seeded Growth

Several nanowire structures were observed after returning to room temperature post experiment which were missing the gold seed particle, see Figure 21.

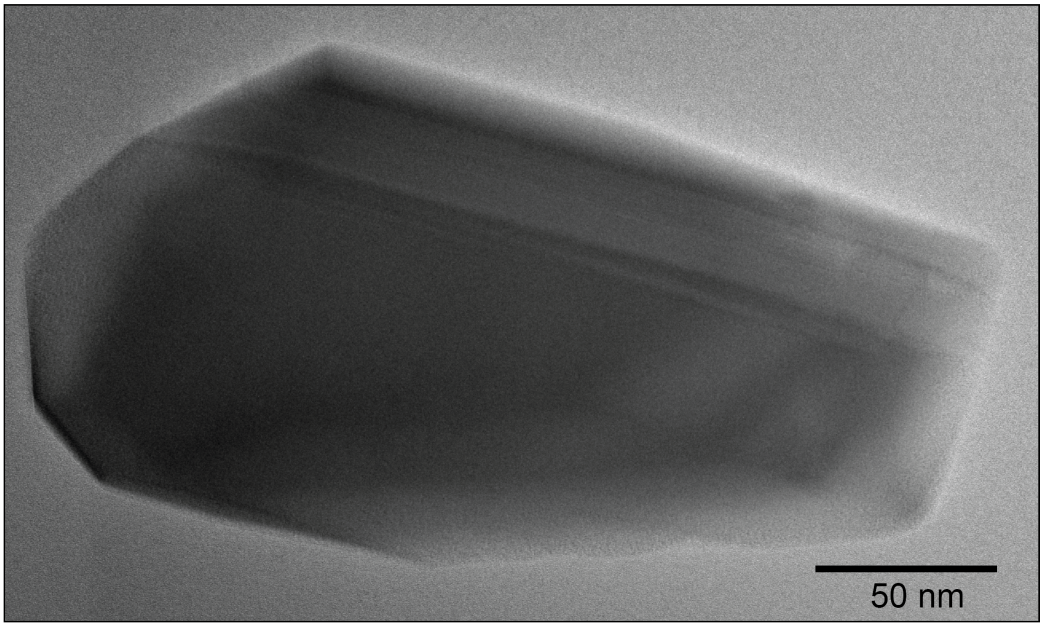

Figure 21: Image of nanowire like structure that is missing the seed particle

Whilst conducting the experiments, some of the droplets either rapidly depleted and shrunk or even disappeared completely when trying to perform XEDS with a focused beam. This suggests that there were several Ga-self-seeded nanowires growing during the experiments, because if the beam was placed on the particle it would rapidly deplete and evaporate. This is explained by relatively high flow of TMGa in the system which was needed in

order to swell the Au seed particles. High partial pressure of TMGa encouraged droplet formation on the SiN_X which were able to nucleate and grow once Sb was introduced in the system. This can be a relevant observation because there are some known issues with using metallic seed particle, mainly elemental contamination. Mostly by using a seed particle, such as Au, there is a risk that either the growing nanowire or the substrate, such as Si, can be contaminated by the elemental Au and create electrically-active deep-levels in the bandgap of the Si nanowire [37]. This means that it destroys the electrical properties of the structure making it unusable. This could be solved by using Ga droplets for the nucleation and growth of GaSb nanowires which would remove the risk of doping. This still needs more research and it is out of the scope of the project. There have been studies which explore self-seeded growth, mainly on GaAs and GaAsSb material systems, but not GaSb [5]. It is important to note that these electrically-active deep-levels have not been observed in GaSb nanowires.

5.2 Tin Seeded Results

In this chapter, results of the Sn seeded experiment are presented. Nucleation conditions and the resulting nanowires are discussed, as well as how the Sn particles behaved during the experiments.

5.2.1 Nucleation Conditions

Au seeded particle nucleation experiments showed that high amount of Ga in the particle is needed in order to nucleate. Thus the same method was followed for the Sn #1 seeded experiment. The experiment with Sn seed particles started by first introducing TMGa into the system in order to let the Sn particle alloy with Ga. The temperature was higher than that of Au experiments, since *ex-situ* studies have shown that Sn seeded GaSb nanowires require higher temperature [7].

The partial pressures for different conditions are presented in Figure 22. The temperature was set to 495°C, but only a small amount of Ga alloyed with the Sn particle. The composition of the seed particle was measured to be 4 at.% Ga and 96 at.% Sn which indicates that either the temperature is too high for Ga to alloy with Sn or that there is not enough Ga in the system. First TMGa flow was increased but it did not result in any more

Ga in the Sn particle, which suggested that temperature might be too high. According to the Ga-Sn phase diagram there is unlimited solubility of Ga in Sn above 231°C but since the phase diagram is constructed for bulk materials it is hard to compare it to nanosize particles [38]. Most likely at elevated temperatures Ga can easily evaporate back to the gas phase, thus reducing the amount of Ga in the particle. It is hard to exactly state what happens at elevated temperatures since the phase diagram temperature limit is 300°C.

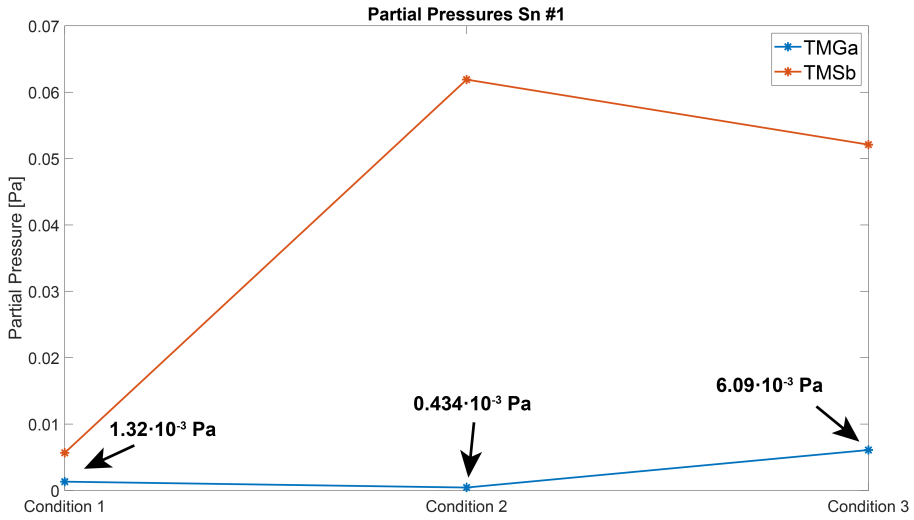

Figure 22: Plot of partial pressures during Sn #1 experiment.

In order to alloy more Ga into the Sn seed particle the temperature was ramped down to 195°C at 5°C per second. During the ramping down it was observed that the Sn particle started to increase in size, meaning that more Ga was present in the particle. At 195°C and at high flows of TMGa there were a lot of Ga droplets forming on the SiN_X substrate. Temperature was increased back again until the Ga droplets on the SiN_X started to evaporate and the composition of the Sn seed particle was measured to be 70 at.% Ga and 30 at.% Sn at 295°C. In order to first try and nucleate at lower amounts of Ga, TMSb was introduced into the system at partial pressures of $1.32 \cdot 10^{-3}$ Pa TMGa and $5.67 \cdot 10^{-3}$ Pa TMSb which is condition 1 in Figure 22. This yielded successful nucleation and the Sn seed particle composition after nucleation remained similar to pre-nucleation at 70 at.% Ga, 28 at.%

Sn and 2 at.% Sb. The nucleated wires had the diameter varying between 25-35 nm, see Figure 23, and were growing at the current conditions, but relatively slowly. In order to increase the growth rate, both TMGa and TMSb flows were increased which led to partial pressure of $4.34 \cdot 10^{-4}$ Pa TMGa and $6.19 \cdot 10^{-2}$ Pa TMSb which is condition 2 in Figure 22. This not only increased the growth rate, but also nucleated most of the particles on the MEMS chip.

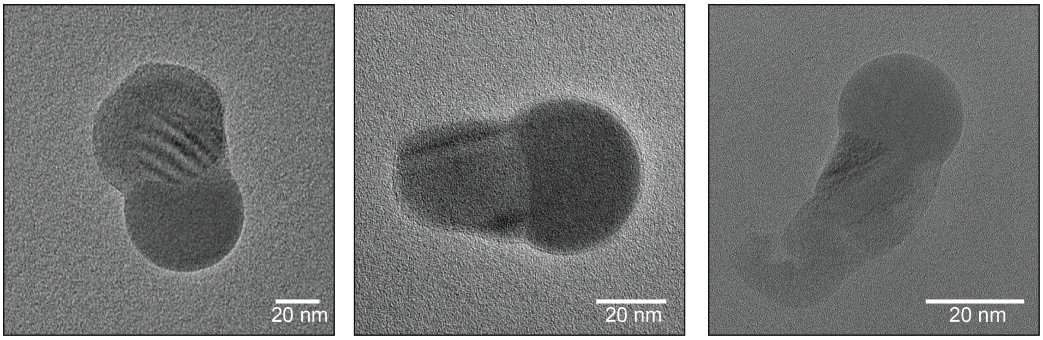

Figure 23: Images of Sn seeded nanowires of varying diameter between 20-30 nm.

Most of the Sn particles were measured to have varying amounts of Ga in the particles ranging from as low as 12 at.% to 70 at.%. To further increase the growth rate of the nanowires temperature was increased to 325°C but this did not affect the growth rate at all, so it was lowered back to 295°C. Instead, TMGa flow was increased, which resulted in partial pressures of $6.09 \cdot 10^{-3}$ Pa TMGa and $5.21 \cdot 10^{-2}$ Pa TMSb which is condition 3 in Figure 22. This further increased the growth rate which suggests that the growth is mass transport limited since temperature does not have any affect. This means that higher total flows of the precursors are needed to achieve higher growth rates [1].

So far nucleation has been achieved by pre-loading with Ga, so in the Sn #2 experiment both TMGa and TMSb were introduced at the same time at molar fractions of $1.19 \cdot 10^{-3}$ TMGa and $1.69 \cdot 10^{-2}$ TMSb. These conditions did not lead to nucleation but when trying to determine the composition of the particle, the beam was focused on the particles which forced most of them to nucleate during the analysis.

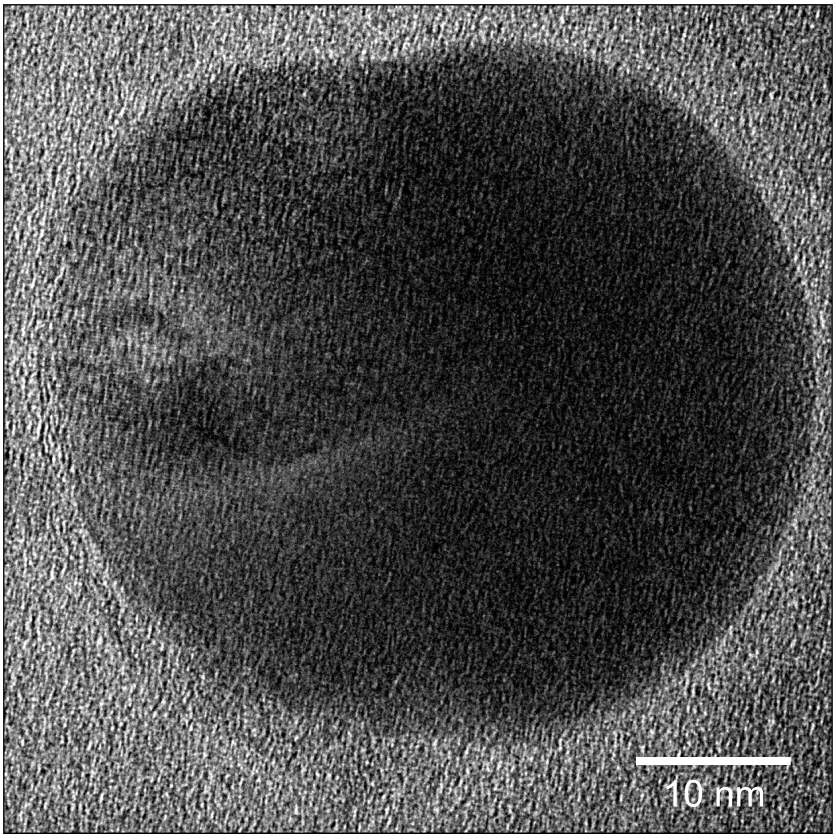

Figure 24: Image of an "exploded" particle. Whilst focusing the beam on the particle to acquire XEDS data, the particle nucleated and crashed but did not grow further.

This lead to skewed quantification data analysis and it was hard to tell the composition of the particle since it now had created a small GaSb crystal nucleus, see Figure 24. After several tries, XEDS analysis was successful without the particle nucleating and the composition was measured to 31 at.% Ga, 54 at.% Sn and 15 at.% Sb. Most likely the particles which did not nucleate during the XEDS analysis were not close enough to the nucleation conditions. It was also observed that particles did not nucleate on their own, but only once the electron beam was focused on them.

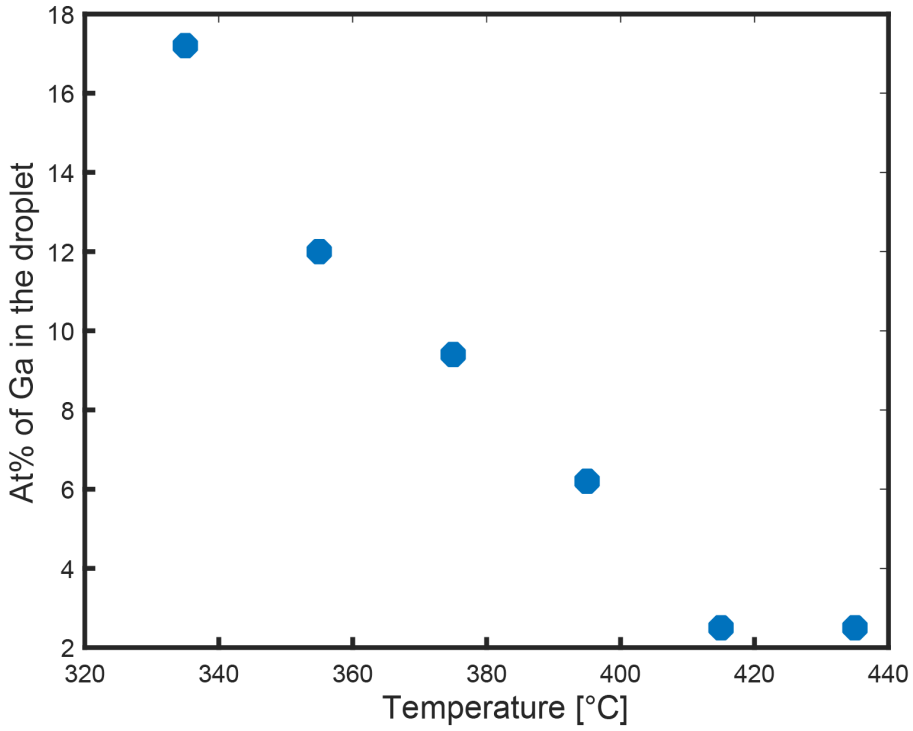

Figure 25: Plot of Ga uptake in the Sn seed particle at different temperatures.

During the Sn #1 experiment it was observed that Ga did not alloy with the Sn particle at elevated temperatures, thus a temperature-composition study was performed for Ga in Sn seed particle during Sn #2 experiment. Temperature was decreased from 420°C to 320°C and the composition was measured which is plotted in Figure 25. Ga started alloying with the Sn particle at 395°C and it started quickly increasing with lower temperature. It was observed that between 340°C and 355°C most of the nanowires started to nucleate, which suggests that the minimum amount of Ga needed in the particle is around 12-16 at.%. The highest amount of Ga in the seed particle was observed to be 70 at.% during the Sn experiments which means that the total range of which Sn seeded particles can nucleate is 12 at.% to 70 at.%.

The yield of successful Sn seeded nucleations is hard to measure, since the partial pressures and temperature were varied during the experiments. When investigating the chips after the experiments, all of the particles seemed to

have nucleated. It is important to note that not all nuclei continued to grow and instead remained relatively small. This suggests that the electron beam might play a role in nucleation and/or that the growth conditions need to be further optimized.

5.3 Au and Sn Comparison

The amount of Ga and Sb needed in the seed particle for nucleation is considerably different for Sn particles compared to Au particles. By using Sn it is possible to nucleate at much lower amounts of Ga and higher amounts of Sb in the droplet. Ga amounts as low as 12 at.% were measured in the droplet during nanowire growth, whilst for Au seeded amount of Ga needed was above 90 at.% in the droplet. This gives a much wider particle composition range for Sn seeded GaSb growth than for Au seeded. Sn seeded nucleation has an upper limit of about 70 at.% whilst Au has the minimum of 90 at.%. By needing high Ga amounts in the particle, the TMGa flow has to be increased which leads to further problems such as large nanowire diameter or excessive deposition and formation of Ga droplets. During the Au experiments there were many big Ga droplets present on the sample, which increased the risk of Au seeded nanowires crashing into them thus rendering them unusable.

Another big difference is the size of particles. Au seeded nanowires ranged from 100 nm to 150 nm in diameter, as shown in Figure 19, which is much larger than what is usually considered as a nanowire. This is an increase of factor 3 from the starting seed particle. By being able to have less amount of Ga in the seed particle, Sn seeded nanowires were much thinner and more reminiscent of conventional nanowire dimensions. This shows more promise if GaSb would be grown *ex-situ* and used for actual electronical devices or other applications.

Sn seeded nanowires nucleate and grow at much lower temperatures compared to gold, which could be an advantage if GaSb would be used industrially. In the industry, output of nanowire fabrication is high, which means it needs great amounts of materials and energy. Since it is possible to nucleate and facilitate nanowire growth from Sn seed at temperatures lower than for Au seed, it would save a lot of energy in heating of the reactor chamber.

One standout observation is that the twin planes were only observed in the big Au seeded nanowire, but none in the Sn seeded experiment. The twin planes most likely formed during the temperature shock, which was not performed on the Sn seeded experiments. This can be just a coincidence and to draw a proper conclusion on if it is easier to induce twin planes in Au or Sn seeded nanowire growth is impossible from this experiment. Further research and investigation is needed in this topic in order to investigate and grow WZ GaSb nanowires.

5.4 Electron Beam Effects

In order to observe the sample during the experiments the electron beam is constantly bombarding the sample with electrons. This leads to unwanted side-effects whilst performing *in-situ* studies. As discussed previously in the Sn particle seeded results part, see Chapter 5.2, some of the the particles nucleated whilst the electron beam was focused on them. This means that every time we are investigating a particle and have the beam focused it can affect the result.

Another side-effect which was observed during the experiments is that quite a lot of contamination was deposited on the parts of the sample where it was exposed to the electron beam for a prolonged amount of time. Mostly it was noticed that at higher flows of TMGa gallium droplets started covering the SiN_X surface of the sample. This is not desired since the small particles can ripen to bigger particles which could be in the way of a growing nanowire. This can be attributed to the electron beam increasing the efficiency of precursor pyrolysis thus creating more local concentrations of material.

A similar effect was also observed when looking at the particles but instead with what is speculated to by hydrocarbons. The high amount of methyl groups present in the system means that it can also be deposited on the sample or the particles themselves. Several of the particles during all the experiments were covered in either an amorphous or graphene like layers which most likely is comprised of carbon. This can hinder and prevent direct nucleations or further growth of the nanowire.

5.5 Aluminum Antimonide

Unfortunately several issues with the ETEMs MOCVD setup meant that proper AlSb experiments could not be performed. However, during one of the Au seeded GaSb experiments we were able to introduce TMAl in the system in order to try and grow AlSb from GaSb. By using a residual gas analyzer it was observed that TMGa was present in the ETEM, even though the TMGa gas flow was closed and only TMAl and TMSb were open. When performing XEDS the composition of the material deposited on the nanowire included not only Ga, Sb, Au, Al but even In. This was attributed to contamination in the bubbler or the gas lines leading to the microscope. During the experiment the microscope was switched to scanning TEM (STEM) in order to image and perform a composition analysis of the resulting structure which is shown in Figure 26. In the STEM composition map it is seen that a signal that is from Al (yellow in the image) which has formed a Al shell around the particle and the structure.

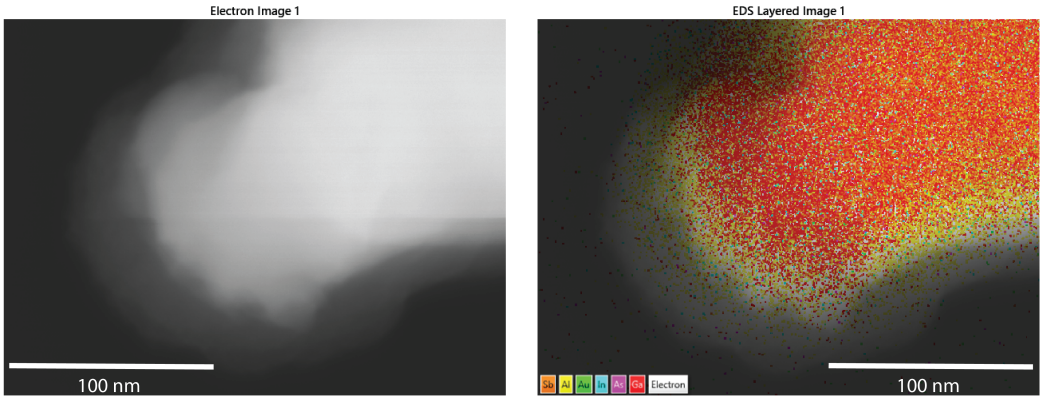

Figure 26: STEM image and composition map of the resulting structure after TMAl was introduced into the system.

6 Conclusions

In this thesis both Au and Sn seeded GaSb direct nucleation was studied. Direct nucleation was achieved by overcoming the supersaturation level in both Au and Sn seed particles. It was shown that a consistent way of nucleating Au seeded GaSb nanowires can be done by varying temperature rapidly - temperature shock. Au seeded nanowires were much wider (100-150

nm) than Sn seeded (25-40 nm), because the amount of Ga needed for nucleation in the Au seed particle was much higher (above 90 at.%) than for Sn seeded (12-70 at.%). This big difference lead to thinner nanowires and much more controllable growth for Sn seeded GaSb compared to Au seeded. A parallel twin plane was observed in one of the Au seeded nanowires which indicates the possibility of other GaSb crystal structures besides ZB, mainly WZ. A temperature range was identified and presented in which Ga can alloy with Sn seed nanoparticles. Lastly, it was observed that the electron beam affected the experiments in several different ways. Firstly, several Sn seeded particles nucleated whilst acquiring XEDS data which suggests that the electron beam can induce nucleation. Secondly, significant hydrocarbon contamination build up was observed at areas which had a prolonged exposure to the electron beam. This was the first time Sn seeded nanowire growth and nucleation was performed in the ETEM at nCHREM. This thesis gives good guidelines on how Sn particles behave, especially when exposed to TMSb and TMGa, so that any upcoming experiments can use the information presented here as a starting point.

7 Outlook

As a summary of this thesis, it is clear that Sn seed particles are more attractive for GaSb nanowire growth. Direct nucleation was relatively easy and consistent, whilst the yield was close to 100%. Although the nucleation was successful, the nanowire growth rate was quite low, thus more work is still required to tune the growth of Sn seeded GaSb.

Since nucleation was easier by using Sn particles, this could suggest that other III-V based nanowires could be grown from Sn instead of other metallic particles such as Au. Parameters such as diameter and structure can be varied more precise by using Sn particles when growing GaSb nanowires. One aspect is also that Sb affect on the particle was much more pronounced in Au seeded nucleation than Sn, which could suggest that other antimony based nanowire growth, such as AlSb, might give better results than with Au seed particles.

Twin planes were observed in Au seeded nanowires, which might indicate

that it is possible to achieve other crystal structures. An interesting study is to see if it is possible to reliably switch between ZB and WZ which could be used to grow heterostructures that could be used as quantum dots. Wurtzite crystal structure in GaSb nanowires has not yet been realized. There have been several theoretical approximation research papers trying to predict how WZ structure bandgap properties compare to the ZB. Most of the models proposed for WZ GaSb have not been able to accurately predict the same parameters, such as band gaps [39][40][41]. Because of the different predictions it is important to further study and research how GaSb could be grown in a WZ crystal structure in order to fully understand the potential of GaSb as III-V material, as well as improving the different theoretical calculations. Also as mentioned previously in this thesis, WZ and ZB have different electrical properties which lends itself to applications such as quantum-dots and electron confinement [20].

A new method of temperature shock for Au seeded nucleation of GaSb nanowires was discovered. This method would allow direct nucleation of GaSb nanowires from different substrates in *ex-situ* by quickly decreasing and then increasing the reactor chamber temperature.

Further research into GaSb nanowires could lend itself useful for other antimonides like AlSb. Finding the optimal conditions which result in stable GaSb nanowire growth can be used to grow a GaSb stem which could be used for AlSb growth thus creating a hetero-structure. This could result in a good overview at what conditions AlSb grows which might lead to direct nucleation of AlSb in the future.

References

[1] Kimberly A. Dick. A review of nanowire growth promoted by alloys and non-alloying elements with emphasis on au-assisted iii–v nanowires. *Progress in Crystal Growth and Characterization of Materials*, 54(3):138–173, 2008.

[2] Ruoxue Yan, Daniel Gargas, and Peidong Yang. Nanowire photonics. *Nature Photonics*, 3(10):569–576, Oct 2009.

[3] Joerg Appenzeller, Joachim Knoch, Mikael T. Bjork, Heike Riel, Heinz Schmid, and Walter Riess. Toward nanowire electronics. *IEEE Transactions on Electron Devices*, 55(11):2827–2845, 2008.

[4] Sergey M. Frolov, Sébastien R. Plissard, Stevan Nadj-Perge, Leo P. Kouwenhoven, and Erik P.A.M. Bakkers. Quantum computing based on semiconductor nanowires. *MRS Bulletin*, 38(10):809–815, 2013.

[5] Enrique Barrigón, Magnus Heurlin, Zhaoxia Bi, Bo Monemar, and Lars Samuelson. Synthesis and applications of iii–v nanowires. *Chemical Reviews*, 119(15):9170–9220, 2019. PMID: 31385696.

[6] B Mattias Borg and Lars-Erik Wernersson. Synthesis and properties of antimonide nanowires. *Nanotechnology*, 24(20):202001, apr 2013.

[7] Marcus Tornberg, Erik K Mårtensson, Reza R Zamani, Sebastian Lehmann, Kimberly A Dick, and Sepideh Gorji Ghalamestani. Demonstration of sn-seeded GaSb homo- and GaAs–GaSb heterostructural nanowires. *Nanotechnology*, 27(17):175602, mar 2016.

[8] Zai-xing Yang, SenPo Yip, Dapan Li, Ning Han, Guofa Dong, Xiaoguang Liang, Lei Shu, Tak Fu Hung, Xiaoliang Mo, and Johnny C. Ho. Approaching the hole mobility limit of gasb nanowires. *ACS Nano*, 9(9):9268–9275, 2015. PMID: 26279583.

[9] Jiamin Sun, Meng Peng, Yushuang Zhang, Lei Zhang, Rui Peng, Chengcheng Miao, Dong Liu, Mingming Han, Runfa Feng, Yandong Ma, Ying Dai, Longbing He, Chongxin Shan, Anlian Pan, Weida Hu, and Zai-xing Yang. Ultrahigh hole mobility of sn-catalyzed gasb nanowires for high speed infrared photodetectors. *Nano Letters*, 19(9):5920–5929, 2019. PMID: 31374165.

[10] Reza R. Zamani, Sepideh Gorji Ghalamestani, Jie Niu, Niklas Sköld, and Kimberly A. Dick. Polarity and growth directions in sn-seeded gasb nanowires. *Nanoscale*, 9:3159–3168, 2017.

[11] Hanna Kindlund, Reza R. Zamani, Axel R. Persson, Sebastian Lehmann, L. Reine Wallenberg, and Kimberly A. Dick. Kinetic engineering of wurtzite and zinc-blende alsb shells on inas nanowires. *Nano Letters*, 18(9):5775–5781, 2018. PMID: 30133288.

[12] Udo W. Pohl. Epitaxy of semiconductors introduction to physical principles graduate texts in physics. 2020.

[13] R. S. Wagner and W. C. Ellis. Vapor-liquid-solid mechanism of single crystal growth. *Applied Physics Letters*, 4(5):89–90, 1964.

[14] Maria E. Messing, Karla Hillerich, Jonas Johansson, Knut Deppert, and Kimberly A. Dick. The use of gold for fabrication of nanowire structures. *Gold Bulletin*, 42(3):172–181, Sep 2009.

[15] Steffen Breuer, Carsten Pfüller, Timur Flissikowski, Oliver Brandt, Holger T. Grahn, Lutz Geelhaar, and Henning Riechert. Suitability of au- and self-assisted gaas nanowires for optoelectronic applications. *Nano Letters*, 11(3):1276–1279, 2011. PMID: 21319838.

[16] Hye Seong Jung, Young Joon Hong, Yirui Li, Jeonghui Cho, Yong-Jin Kim, and Gyu-Chul Yi. Photocatalysis using gan nanowires. *ACS Nano*, 2(4):637–642, 2008. PMID: 19206593.

[17] J. Y. Marzin, J. M. Gérard, A. Izraël, D. Barrier, and G. Bastard. Photoluminescence of single inas quantum dots obtained by self-organized growth on gaas. *Phys. Rev. Lett.*, 73:716–719, Aug 1994.

[18] Sepideh Gorji Ghalamestani, Sebastian Lehmann, and Kimberly A. Dick. Can antimonide-based nanowires form wurtzite crystal structure? *Nanoscale*, 8:2778–2786, 2016.

[19] Chin-Yu Yeh, Su-Huai Wei, and Alex Zunger. Relationships between the band gaps of the zinc-blende and wurtzite modifications of semiconductors. *Phys. Rev. B*, 50:2715–2718, Jul 1994.

[20] Irene Geijselaers, Neimantas Vainorius, Sebastian Lehmann, Craig E. Pryor, Kimberly A. Dick, and Mats-Erik Pistol. Atomically sharp, crystal phase defined gaas quantum dots. *Applied Physics Letters*, 119(26):263102, 2021.

[21] C.B. Williams, D.B Carter. Transmission electron microscopy - a textbook for materials science 2nd springer science. 2009.

[22] R.F. Egerton. Physical principles of electron microscopy. *Phys. Rev. B*, 50, 2016.

[23] Jiantao Zhang, Xiaojun Hu, and Kuochih Chou. In-situ environmental transmission electron microscopy investigation of the phase transformation austenite → ferrite in duplex stainless steel. *Materials Letters*, 264:127259, 2020.

[24] Yi-Chia Chou, Federico Panciera, Mark C. Reuter, Eric A. Stach, and Frances M. Ross. Nanowire growth kinetics in aberration corrected environmental transmission electron microscopy. *Chem. Commun.*, 52:5686–5689, 2016.

[25] Carina B. Maliakkal, Erik K. Mårtensson, Marcus Ulf Tornberg, Daniel Jacobsson, Axel R. Persson, Jonas Johansson, Lars Reine Wallenberg, and Kimberly A. Dick. Independent control of nucleation and layer growth in nanowires. *ACS Nano*, 14(4):3868–3875, 2020. PMID: 32049491.

[26] A. K. Erdamar, S. Malladi, F. D. Tichelaar, and H. W. Zandbergen. *Closed Cell Systems for In Situ TEM with Gas Environments Ranging from 0.1 to 5 Bar*, pages 165–210. Springer International Publishing, Cham, 2016.

[27] Crispin Hetherington, Daniel Jacobsson, Kimberly A Dick, and L Reine Wallenberg. In situ metal-organic chemical vapour deposition growth of iii–v semiconductor nanowires in the lund environmental transmission electron microscope. *Semiconductor Science and Technology*, 35(3):034004, feb 2020.

[28] Larry Lesyna, Don Di Marzio, Stephen Gottesman, and Martin Kesselman. Advanced x-ray detectors for the analysis of materials. *Journal of Low Temperature Physics*, 93(3):779–784, Nov 1993.

[29] Marcus Tornberg, Carina B. Maliakkal, Daniel Jacobsson, Reine Wallenberg, and Kimberly A. Dick. Enabling in situ studies of metal-organic chemical vapor deposition in a transmission electron microscope. *Microscopy and Microanalysis*, 28(5):1484–1492, 2022.

[30] Jan-Olle Malm Jan-Olov Bovin Martin H. Magnusson, Knut Depert and Lars Samuelson. Size-selected gold nanoparticles by aerosol technology. 1999.

[31] Martin H. Magnusson, Knut Deppert, Jan-Olle Malm, Jan-Olov Bovin, and Lars Samuelson. Gold nanoparticles: Production, reshaping, and thermal charging. *Journal of Nanoparticle Research*, 1(2):243–251, Jun 1999.

[32] Robin Sjökvist, Marcus Tornberg, Mikelis Marnauza, Daniel Jacobsson, and Kimberly A. Dick. Observation of the multilayer growth mode in ternary ingaas nanowires. *ACS Nanoscience Au*, 2(6):539–548, 2022.

[33] Marcus Tornberg, Robin Sjökvist, Krishna Kumar, Christopher R. Andersen, Carina B. Maliakkal, Daniel Jacobsson, and Kimberly A. Dick. Direct observations of twin formation dynamics in binary semiconductors. *ACS Nanoscience Au*, 2(1):49–56, 2022.

[34] John McGinty, Nima Yazdanpanah, Chris Price, Joop H. ter Horst, and Jan Sefcik. Chapter 1 nucleation and crystal growth in continuous crystallization. In *The Handbook of Continuous Crystallization*, pages 1–50. The Royal Society of Chemistry, 2020.

[35] Dasa L. Dheeraj, Gilles Patriarche, Hailong Zhou, Thang B. Hoang, Anthonysamy F. Moses, Sondre Grønsberg, Antonius T. J. van Helvoort, Bjørn-Ove Fimland, and Helge Weman. Growth and characterization of wurtzite gaas nanowires with defect-free zinc blende gaassb inserts. *Nano Letters*, 8(12):4459–4463, 2008. PMID: 19367852.

[36] Mattias Jeppsson, Kimberly A. Dick, Jakob B. Wagner, Philippe Caroff, Knut Deppert, Lars Samuelson, and Lars-Erik Wernersson. Gaas/gasb nanowire heterostructures grown by movpe. *Journal of Crystal Growth*, 310(18):4115–4121, 2008.

[37] Deepak Sharma, Abhishek Motayed, Sergiy Krylyuk, Qiliang Li, and Albert V. Davydov. Detection of deep-levels in doped silicon nanowires using low-frequency noise spectroscopy. *IEEE Transactions on Electron Devices*, 60(12):4206–4212, 2013.

[38] Ga-sn binary phase diagram 0-100 at.% sn: Datasheet from "pauling file multinaries edition – 2012" in springermaterials (https://materials.springer.com/isp/phase-diagram/docs/c_0902787). Copyright 2016 Springer-Verlag Berlin Heidelberg & Material Phases

Data System (MPDS), Switzerland & National Institute for Materials Science (NIMS), Japan.

[39] M. Murayama and T. Nakayama. Chemical trend of band offsets at wurtzite/zinc-blende heterocrystalline semiconductor interfaces. *Phys. Rev. B*, 49:4710–4724, Feb 1994.

[40] Martin Gmitra and Jaroslav Fabian. First-principles studies of orbital and spin-orbit properties of gaas, gasb, inas, and insb zinc-blende and wurtzite semiconductors. *Phys. Rev. B*, 94:165202, Oct 2016.

[41] Abderrezak Belabbes, Christian Panse, Jürgen Furthmüller, and Friedhelm Bechstedt. Electronic bands of iii-v semiconductor polytypes and their alignment. *Phys. Rev. B*, 86:075208, Aug 2012.